Waveform Selection For Multi-Band Multistatic Radar Networks

WAVEFORM SELECTION FOR MULTI-BAND MULTISTATIC RADAR NETWORKS

Murat Temiz, Matthew Ritchie, Hugh Griffiths
Department of Electronic and Electrical Engineering
University College London, London

ABSTRACT

This study investigates the benefits of waveform selection by exploiting multiple illuminators of opportunity (IO) in hybrid radar systems consisting of multi-band receivers which can utilise active radar transmitters and broadcasting signals for bistatic radar sensing. As a performance metric, Cramér-Rao lower bounds (CRLBs) on velocity and range estimations are considered. Considering that TV and radio broadcasting stations usually emit high power signals, they are suitable for passive sensing as IOs. Therefore, FM radio, Digital Video Broadcasting-Terrestrial (DVB-T) and Digital Audio Broadcasting (DAB) transmitters are considered for passive radar operations while also having an active radar transmitter in the multistatic radar network. Multistatic radar networks comprising receivers, transmitter and IOs transmitting the aforementioned waveforms are modelled and optimum selection of bistatic pairs are studied based on CRLBs on range and velocity estimations. Two different multistatic radar network scenarios are simulated and the results are evaluated to analyse the estimation accuracy of active and passive bistatic pairs in the network. The results show that multi-band multistatic radar network provides better range and velocity estimations and may also mitigate the adverse effects of jamming by exploiting broadcasting waveforms compared to a radar network which only considers radar transmitters for sensing.

1 Introduction

bluePassive radar systems make use of broadcasting, communications or radio navigation transmissions (e.g., TV or radio signals) as illuminators of opportunity (IOs) for target detection rather than having dedicated radar transmitters [1]. Passive radar is also known as passive bistatic radar (PBR) since the broadcasting stations and receivers can be in different locations [2]. PBR is especially attractive for stealth and low-cost sensing or experimental research applications since it does not require any transmitter (Tx) and only a receiver (Rx) equipped with surveillance and reference antennas is sufficient for radar measurements. blueMoreover, passive radar has been recently considered for cognitive radar applications due to its stealth and multi-waveform sensing abilities [3]. Meanwhile, broadcasting or communication signals are not specifically designed for radar operations and their properties vary over time depending on the data transmitted, and this affects the sensing performance. Furthermore, in active or passive bistatic radar systems, the bistatic geometry between the Tx-target-Rx pairs significantly impacts the accuracy of target detection and parameter estimation. Therefore, the geometry of the radar network must be considered in addition to waveform properties blueand received signal power while evaluating the performance of passive or active bistatic radar systems [4].

In this study, we consider a hybrid multi-band multistatic radar network consisting of an active radar transmitter and also utilises passive IOs available in the area of interest to provide an enhanced target parameter estimation. Since the bistatic geometry significantly impacts the parameter estimation, the optimum Tx-Rx pair for achieving the best estimation accuracy chiefly depends on the location of the target [5]. Consequently, although an active radar sensing is expected to outperform passive radar sensing in most cases, passive bistatic pairs may perform better for some specific target locations depending on the bistatic geometry, signal-to-noise ratio (SNR) or signal-to-interference-plus-noise (SINR). Moreover, in some cases, the active radar system may want to switch off its transmitter to reduce its detectibility. In order to make this decision, the knowledge of active radar performance versus passive radar performance is required. blueTherefore, the purpose of this study is to investigate the theoretical performance limits

of multi-waveform hybrid multistatic radar networks since multi-waveform receivers, which can exploit broadcasting signals and radar waveforms for sensing, have been recently developed and implemented such as in [6, 7, 8]. However, the theoretical performance limits of multi-waveform multistatic radar networks consisting of such receivers have not been systematically investigated. Therefore, this study aims to fill this gap in the literature by modelling such networks and utilising CRLBs on the range and velocity estimations to quantitatively show the advantages of using such receivers and hybrid multistatic radar networks.

Various broadcast or communication waveforms have been considered as illuminators of opportunity (IO) for passive radar sensing. Among these, FM radio, Digital Video Broadcasting-Terrestrial (DVB-T) and Digital Audio Broadcasting (DAB) signals are desirable ones for long-range sensing applications due to their wide area coverage, high transmit power, sufficient bandwidth and well-known bluewaveform structures [6, 9]. FM radio signals have been considered for passive radars especially because of their high transmit power, low path-loss transmission due to their low carrier frequency and widely availability around the world. Although the range resolution of FM signals are limited due to their narrow band and highly content-dependent spectrum, they can be effectively utilised for estimating target velocity [7]. Multi-band passive radar receivers utilising broadcasting signals were successfully developed, implemented and tested in real-time measurements [8, 7]. For examples, a multi-band passive radar system utilising FM and DVB-T signals were developed and tested in a real scenario [7], where 4 seconds coherent processing interval (CPI) was chosen for FM radio signals with average 80 kHz bandwidth while the DVB-T based PBR system exploited one DVB-T frame with 7.7 MHz bandwidth for sensing. The range resolution of the FM based PBR was relatively large, between 2 and 3 km throughout the measurements, but it delivered a fine Doppler resolution of 0.25 Hz. The range resolution achieved by the DVB-T based PBR system was around 40 times finer than the FM based PBR system but DVB-T system demonstrated a coarser Doppler resolution, i.e., 4.23 Hz, due to the reduced observation duration. In another study, a mobile multi-band multi-illuminator system utilising available FM radio, DAB and DVB-T signals for passive sensing was developed and tested to detect the targets for airspace surveillance in a very wide area [8], in which the passive radar system was built on a van for mobility. The measurement results showed that it is possible to achieve 30 m range accuracy via fusion of FM, DAB and DVB-T signal opportunities. This study also shows that there might be multiple transmitters of each broadcast system in the area, therefore, it is possible to cover a wide area for sensing by utilising more IOs. Moreover, FM radio and DVB-T based PBR systems were also considered for airborne radars due to their small size, light structure, low power consumption, and stealth operation abilities [10]. On the other hand, for short-range passive radar sensing applications, WiFi and cellular network signals have also been considered [11, 12, 13].

In a PBR system, in addition to the surveillance signals reflected off the targets, the reference signal from the non-cooperative transmitter needs to be acquired for radar signal processing via a directional reference antenna which is directed towards the non-cooperative transmitter. However, this signal also includes noise as much as the noise the surveillance signal has. One of the solutions for removing the noise in the reference signal is to demodulate and reconstruct the reference signal if the modulation type of this signal is known [14]. This signal reconstruction was shown to improve the detection performance in DVB-T passive radar systems when the SNR of the reference signal is sufficient for highly accurate demodulation [14]. However, for low SNR signals, demodulation of the reference signal will include significant errors, therefore, signal reconstruction techniques may not work well due to the demodulation errors [15, 14].

Cramér–Rao lower bounds (CRLBs) have been widely used in radar studies to evaluate the detection performance of various radar systems and waveforms and also used as a benchmark for parameter estimation algorithms as it defines the lower bounds of mean squared error (MSE) of the estimation, i.e., achievable best estimation accuracy, for unbiased estimators. [16, 17]. Efficient unbiased estimators can attain CRLBs, for instance, maximum likelihood estimator (MLE) was shown to reach the CRLBs when the received radar returns have sufficient SNR [18]. Furthermore, the CRLB can be calculated for different parameter estimations such as velocity, range, angle, location estimations, and this makes the CRLB a commonly used benchmark for estimator studies [16, 19, 17, 20, 21]. blueFor example, it was shown that efficient target tracking and localisation algorithms can achieve the minimum variance, as defined by the CRLBs [22, 23]. The minimum mean squared error (MSE) is equal to the square root of the CRLBs if the estimator is unbiased and efficient such as maximum likelihood estimator (MLE) as shown via simulations in [20], or maximum a posteriori estimation (MAP) as shown in [24]. Therefore, CRLBs on the range and velocity estimations are utilised as performance metrics to evaluate the performance of different Tx-Rx pairs in this study.

While CRLBs on target parameter estimations are only functions of SNR (or SINR) and radar waveform in monostatic radar systems [25], bistatic geometry has an significant impact on the CRLBs in bistatic radar networks [5]. Consequently, CRLBs in bistatic and multistatic radar networks were previously extensively studied by considering various waveforms such as FM radio signals [9, 26], OFDM communication signals [27, 20, 28], linear frequency modulated (LFM) waveforms [5], advanced television system committee (ATSC) signals [29], and mobile communication network signals [30]. It is also possible to compute joint CRLBs such as for joint delay and Doppler estimations in

multi-target scenarios [31]. blueFurthermore, the CRLB has been recently considered as a performance metric in a joint radar and communication system while optimising the joint system performance. [32].

Unlike the aforementioned studies, instead of considering a single type of IO, this study considers multiple waveforms possibly available in the area of interest to improve range and velocity estimations for different target locations. Multi-band receivers equipped with multiple surveillance and reference antennas are placed at different locations so that the range and velocity estimations are overall improved in the multistatic radar network. Such multi-band multi-illuminator passive radar receivers have already been developed, implemented and measured to evaluate their performance [8, 7] which demonstrate that FM, DAB, DVB-T can be jointly and efficiently utilised for passive bistatic sensing. There are significant advantages of utilising multiple sources operating at different frequency bands. Firstly, utilising different frequencies and broadcast technologies such as FM radio and DVB-T signals in addition to active radar sensing results in a substantially more robust radar system against any potential jamming since multi-band jamming is not an easy task and the jammer does not probably know which frequencies are used for passive sensing. Secondly, the active transmitter may be switched off anytime to enable passive sensing by jointly utilising non-cooperative illuminators. Thirdly, since the non-cooperative illuminators are probably distributed in the area, the impact of bistatic geometry on the bistatic sensing may be mitigated by selecting optimum Tx-Rx pairs for different target locations [33]. Such multi-band multistatic active and passive radar networks can be used for ground-based air surveillance systems or airborne radar systems to create cognitive radar platforms which can also perform stealth sensing when it is necessary. Therefore, in this study, in addition to utilising multiple broadcasting waveforms, we also consider an X-band active radar system which is widely used in ground-based surveillance and airborne radar systems due to its small antenna dimensions, sufficient bandwidth, fine range resolution, good coverage and robustness to weather conditions [34]. blueConsequently, the main contributions of this study are:

1. blueThis study considers multiple types of IOs (multi-waveform) for hybrid (active/passive) multistatic radar sensing in order to analyse CRLBs on the range and velocity estimations in more realistic radar network scenarios since it is possible to utilise different waveforms via multi-waveform passive radar receivers. In comparison, previous literature has only focused on single waveform IOs for range and velocity estimations and provided CRLBs analysis for a single waveform type in multistatic networks. For example, FM radio signals in [9], LFM waveform in [5] and OFDM signals in [28] were considered.
2. blueBy analysing the CRLBs with regards to the multistatic network geometry and various radar waveforms, it shows that intelligently utilising multiple different IOs greatly enhances radar sensing performance by complementing the active radar sensing without transmitting any additional radar waveform. Moreover, it shows that passive bistatic sensing might be desirable in some parts of the network since the active bistatic sensing might encounter the forward scatter situation due to the geometry between the transmitter, target and receiver.
3. blueIt proposes a waveform selection method based on the CRLBs on the range and velocity estimations to maximise the target parameter estimation accuracy. For this aim, it calculates the CRLBs of the entire area of interest in advance so that the most suitable waveform for a specific target location can be selected. Furthermore, it shows that different pairs might be desirable for velocity and range estimations of the same target since each waveform has different characteristics for range and velocity estimations due to the bandwidth and carrier frequency in addition to bistatic geometry. Therefore, it is important to model the entire hybrid multistatic radar network to determine the optimum pairs for velocity and range estimations. The decision on which waveform to select at any one moment should be evaluated via CRLBs to ensure the maximum performance throughout a scenario. If only the waveform parameters alone utilised to make this decision, degraded performance will occur. Based on this information, a novel waveform selection process based on CRLB is described within this paper.

In the rest of the paper, Section 2 presents the system model, while Section 3 discusses the monostatic ambiguity function and CRLBs of LFM, FM radio and OFDM waveforms. In Section 4, the bistatic CRLBs expressions for range and velocity estimations are presented. Section 5 summarises the waveform selection process for the maximum performance whereas Section 6 evaluates two different multi-band multistatic radar network scenarios and compares their performance in terms of CRLBs and shows the importance of waveform selection. Finally, Section 7 draws the conclusions.

2 System Model

In the multistatic radar network under consideration, the receivers are assumed to have multiple surveillance and reference antennas operating at FM radio, DVB-T, DAB and active radar frequencies to be able to utilise different IOs for sensing. In this research, it is assumed that the active radar transmitter and receivers are cooperative, synchronised

and utilise LFM waveform. However, the instantaneous properties of the transmitted waveforms by FM radio, DVB-T and DAB stations are not known, therefore, the receivers have also reference antennas to acquire the reference signals from these sources.

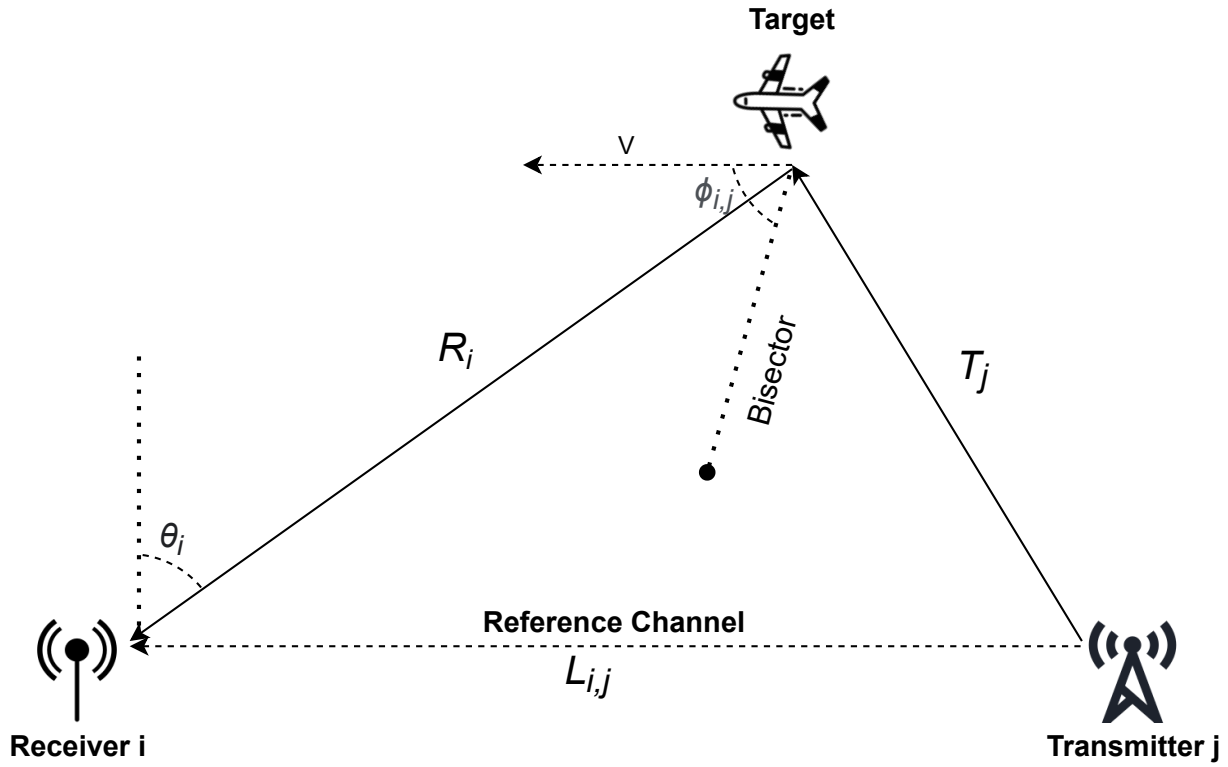

Figure 1: Illustration of the bistatic geometry between the jth transmitter, target and ith receiver.

The multistatic radar network under consideration consists of J transmitters, I receivers and a single target for the sake of simplicity. The distance between the jth transmitter and the ith receiver (i.e., baseline) is denoted by $L_{i,j}$ and the distance between the target and the jth transmitter is denoted by T_j and the distance between the target and the ith receiver is denoted by R_i as shown in Fig. 1. The angle between the receiver and target is defined by θ_i, and the angle of the target velocity vector to the bistatic bisector is defined by $\phi_{i,j}$. Therefore, the relative velocity of the target is calculated as $V_{i,j} = V \cos \phi_{i,j}$, where V denotes the velocity of the target. Transmitters, targets and receivers are placed at (x_j, y_j, z_j), (x_t, y_t, z_t), (x_i, y_i, z_i) points, respectively in the multistatic network, represented by a 3D coordinate system. Therefore, all of the parameters mentioned above can be calculated for all bistatic pairs using these coordinates in the simulations. Moreover, B_j and f_j denote the bandwidth and carrier frequency of the waveform transmitted by the jth transmitter.

For each Tx-target-Rx pair, the received signal at the ith surveillance antenna from the jth transmit antenna after reflecting from a single target is given by

$$\begin{aligned} x_{ij}(t) = &\sqrt{\xi_{i,j}(t)} u_j(t - \tau_r) \\ &+ \sqrt{\alpha_{i,j}(t)\,\sigma_t} u_j(t - \tau)\, e^{-j2\pi\omega(t)} + n_i(t), \end{aligned} \tag{1}$$

where $u_j(t)$ is the transmitted waveform by the jth transmitter, $\alpha_{ij}(t)$ denotes the total channel gain which consists of transmit power, antenna gains and path loss, σ_t denotes the RCS of the target, and $n_i(t) \sim \mathcal{CN}\left(0, \sigma_i^2\right)$ is the AWGN noise at the ith surveillance antenna receiver. The delay caused by the target range and the Doppler frequency caused by the target velocity are denoted by τ and ω, respectively. Moreover, the delay in the reference channel is denoted by τ_r, and the direct-path interference (DPI) is denoted by $\xi_{i,j} u(t - \tau_r)$ where $\xi_{i,j}$ is the blueproduct of the transmit power, antenna gain and path loss of the direct path between the jth transmit antenna and the ith surveillance receive antenna. The transmitters and IOs are assumed to operate with different carrier frequencies, therefore, any interference between them is not considered.

In the case of passive radar, the reference signal is acquired by a reference antenna as given by [35]

$$y_{i,j}(t) = \sqrt{\psi_{i,j}(t)} u_j(t - \tau_r) + n_{r,i}(t), \tag{2}$$

where $\psi_{i,j}$ denotes the sum of transmit power, antenna gain and path loss of the direct path between the jth transmit antenna and the ith reference receive antenna and $n_{r,i}(t)$ denotes the noise at the reference antenna receiver. The reference antenna is usually directed to the transmitter to maximize the gain of the reference signal while the surveillance antenna should be isolated from the direct path signals, hence, $\psi_{i,j} > \xi_{i,j}$ can be given. Furthermore, considering that surveillance and reference antenna receivers have the same bandwidth, $n_{r,i}(t) = n_i(t)$ is accepted. When SNR of the reference channel is sufficiently high, the impact of the noise in the reference channel is negligible, however, in low SNR cases, it affects the target parameter estimation [36]. Taking into account both the noise in the reference and surveillance channels, the signal-to-interference-noise-ratio (SINR) of the received signal can be approximated by

$$\rho_{i,j} = \frac{\alpha_{i,j}(t)\sigma_t}{2\sigma_i^2 + \mu_{DPI}\xi_{i,j}(t)}, \tag{3}$$

where $0 \leq \mu_{DPI} \leq 1$ denotes the residual DPI ratio after DPI cancellation since passive radar systems employ DPI cancellation algorithms [37] such as Wiener or least squares (LS) filters [29]. Therefore, parameter μ_{DPI} is used to express the effectiveness of the DPI cancellation algorithm. For instance, $\mu_{DPI} = 0$ indicates that the DPI is entirely canceled while $\mu_{DPI} = 0.1$ indicates that 90% of the DPI is cancelled. Various DPI cancellation methods are reviewed in [38]. For example, DPI cancellation may reach up to 80 dB suppression performance by utilising a least squares (LS) filter with a large number of filter taps [38]. For the active bistatic radar case, SINR is given by $\rho_{i,j} = \frac{\alpha_{i,j}(t)\sigma_t}{\sigma_i^2}$ since the transmitted waveform is known, therefore, it does not require a reference antenna. Parameters $\alpha_{i,j}$, $\psi_{i,j}$ and $\xi_{i,j}$ are calculated using the radar and path-loss equations as in [29].

The noise variance at the ith receiver is modeled as $\sigma_i^2 = k_B T_0 B_i N_F$, where k_B, T_0 and N_F denote the Boltzmann's constant (1.38×10^{-23} J/K), reference temperature (290 K) and receiver noise figure in linear scale. Note that noise in the reference channel can be removed by reconstructing the reference signal in DVB-T and DAB systems since the received signal can be demodulated and then re-modulated to acquire the reference signal without noise [14]. While this method can efficiently reconstruct the reference signal when the SNR is sufficiently high, it is not beneficial in low SNR cases as a significant amount symbols will be erroneously demodulated when the SNR is not sufficient.

3 Monostatic Ambiguity Function and Cramér-Rao Lower Bounds

Performance of a bistatic radar has been demonstrated to be mainly related to the bistatic geometry, SINR and transmitted waveform [1]. Therefore, it is paramount to understand waveform-related parameters, namely monostatic ambiguity function and CRLBs in addition to the bistatic geometry of the Tx-target-Rx pair. It was shown that monostatic CRLBs on range and velocity estimations can be derived from the monostatic ambiguity functions of waveforms [39, 25, 40]. For a waveform defined by $u(t)$, the ambiguity function is given by [39]

$$|\Omega(\tau, \omega)| = \left| \int_{-\infty}^{+\infty} u(t) u^*(t - \tau) e^{-j2\pi\omega t} dt \right|, \tag{4}$$

where τ and ω denote delay and Doppler frequency, respectively. The monostatic CRLBs of waveform $u(t)$ is calculated via the monostatic Fisher information matrix (FIM) of which elements are related to the ambiguity function of the waveform [28, 5, 25]. The monostatic FIM for the delay and Doppler estimation is given by [5]

$$\mathbf{J}_M(\tau, \omega) = -2\rho\mathbf{J}_0 = -2\rho \begin{bmatrix} \frac{\partial^2 \Theta(\tau,\omega)}{\partial \tau^2} & \frac{\partial^2 \Theta(\tau,\omega)}{\partial \tau \partial \omega} \\ \frac{\partial^2 \Theta(\tau,\omega)}{\partial \omega \partial \tau} & \frac{\partial^2 \Theta(\tau,\omega)}{\partial \omega^2} \end{bmatrix}, \tag{5}$$

where $\Theta(\tau, \omega) = |\Omega(\tau, \omega)|^2$, and $\mathbf{J}_0$ is a matrix which only consists of partial derivatives of the waveform related parameters without SNR or SINR. Matrix $\mathbf{J}_0$ will be given in the next subsections for each waveform considered in this study, i.e., $\mathbf{J}_{(LFM)}$ for LFM, $\mathbf{J}_{(SFM)}$ for FM radio and $\mathbf{J}_{(OFDM)}$ for OFDM signals. After computing the FIM, the monostatic CLRBs on delay and Doppler frequency can be respectively calculated by [5, 39]

$$\mathrm{CRLB}(\tau) = \left[\mathbf{J}_M^{-1}(\tau, \omega)\right]_{1,1}, \tag{6}$$

$$\mathrm{CRLB}\left(\omega\right) = \left[\mathbf{J}_M^{-1}\left(\tau,\omega\right)\right]_{2,2}. \tag{7}$$

In this study FM, DAB and DVB-T signals are utilized for passive sensing in addition to active radar waveform LFM. While FM radio signals are modulated using sinusoidal frequency modulation (SFM), DAB and DVB-T signals are modulated with OFDM. Therefore, CRLBs of these modulations schemes will be presented in the next subsections.

3.1 LFM Waveform

LFM is widely used in radar applications due to its low-cost hardware requirements, computationally efficient processing and excellent Doppler properties [41]. The complex-valued LFM waveform is given by [5]

$$u_{LFM}\left(t\right) = \begin{cases} Ae^{j\pi kt^2} & 0 \le t \le T_p \\ 0 & else \end{cases}, \tag{8}$$

where blue A denotes the amplitude of the pulse, and $k = B/T_p$ denotes the relation between the LFM pulse bandwidth, $B = f_1 - f_0$, and pulse duration T_p. Analytical CRLB expressions for LFM bursts are derived and used in various studies [5, 25, 39]. The elements of FIM matrix for delay and Doppler measurements with N LFM pulses is given by [5]

$$\mathbf{J}_{LFM} = \begin{bmatrix} \frac{-k^2\pi^2T_p^2}{3} & \frac{k\pi^2T_p^2}{3} \\ \\ \frac{k\pi^2T_p^2}{3} & \frac{\pi^2T_R^2\left(1-N^2\right)-\pi^2T_p^2}{3} \end{bmatrix}, \tag{9}$$

where B, T_p, T_R and N denote the bandwidth, duration of each pulse, pulse repetition interval and number of LFM pulses. The details of the FIM and CRLBs derivations of LFM waveforms can be found in [25, 5].

3.2 FM Radio Signals

FM radio signals have been widely utilised in passive radar systems because FM stations have high output power resulting in a very wide coverage area which makes it suitable for long-range passive radar applications. The major drawback of FM radio signals is their narrow and continuously varying bandwidth depending on the instantaneous content of the channel. This leads very coarse delay estimation, hence, range resolution. However, FM radio signals can provide sufficient Doppler frequency estimation, hence, velocity resolution with a reasonably selected observation time for passive sensing. Moreover, the transmit power of FM radio transmitters is higher compared to other broadcasting technologies and it transmits using a lower carrier frequency, resulting in a very wide coverage and sufficient SNR for passive sensing. FM signals are modulated using analogue sinusoidal frequency modulation (SFM) technique. Since its frequency varies over time, it is not possible to give an exact model of FM radio signals, therefore, an approximate model of FM radio signals over observation duration T is given by [33]

$$u_{SFM}\left(t\right) = \begin{cases} \frac{A}{\sqrt{T}}e^{j\beta sin(2\pi f_0 t+\phi)} & 0 \le t \le T \\ 0 & else \end{cases}, \tag{10}$$

where approximate bandwidth of the signal is expressed by Carson's bandwidth as $B_c = 2(\delta f + f_m) = 2\beta f_0$, and δf and f_m denote the peak frequency deviation and the highest frequency in the modulation signal, and ϕ denotes the phase [33]. Since characteristics of FM radio signals are related to the instantaneous content of the radio channel, there is not any exact analytical FIM and CRLBs expressions for this waveform. However, modified FIM expressions are derived based on the approximate signal model given by (10) as [33]

$$\mathbf{J}_{SFM} = \begin{bmatrix} 4\pi^2\beta^2f_0^2 & -\left(-1\right)^z 2\pi\beta\sin\left(\phi\right) \\ \\ -\left(-1\right)^z 2\pi\beta\sin\left(\phi\right) & \frac{\pi^2T^2}{3} \end{bmatrix}, \tag{11}$$

where $z = Tf_0$ is an integer and denotes the number of SFM pulses observed.

3.3 DVB-T and DAB Signals

DVB-T and DAB signals have also been exploited as IOs for passive radar systems since they are broadcasted with a high power ($\geq$ 5 kW) to cover wide areas and available in most countries [42, 43]. Moreover, DVB-T channels have

sufficient bandwidth to deliver a reasonable range resolution. Its delay and Doppler properties were well investigated and signal processing techniques to alleviate the effects of the ambiguities and the clutter on the radar image were proposed [44]. Both DVB-T and DAB broadcasting standards utilised coded OFDM (COFDM) scheme but with different parameters such different subcarrier spacings, bandwidths, symbol durations and cyclic-prefix durations. OFDM is widely employed in modern communication systems since it overcomes multi-path fading effects while maximising the spectral efficiency by dividing a wideband channel into narrow band sub-channels. Moreover, it is possible to perform radar sensing using OFDM waveforms via signal processing techniques as explained in [45, 46]. Although different countries have different DVB-T and DAB standards, it is widely accepted that the bandwidth of DVB-T and DAB channels are 7.61 MHz and 1.536 MHz, respectively. DVB-T/DVB-T2 standards have various modes depending on the subcarrier spacing but all modes have the same effective bandwidth of 7.61 MHz in 8 MHz channels. 2K and 8K DVB-T modes are generally considered for passive sensing [47]. Because of the bandwidth difference between DVB-T and DAB signals, DVB-T signals provide significantly finer range resolution compared to DAB signals while their velocity resolutions are expected to be similar for the same observation duration.

The lth OFDM symbol consisting of N_s subcarriers is given by [28]

$$u_l(t) = \begin{cases} \sum_{n=-N_s/2}^{N_s/2-1} A s_{n,l} e^{j2\pi n \Delta f (t-T_{cp})} & 0 \le t \le T_{sym} \\ 0 & else \end{cases}, \tag{12}$$

where $s_{n,l}$ denotes the lth QAM symbol transmitted in the nth subcarrier. Moreover, $\Delta f, T_{sym}, T_{cp}$ denote the OFDM subcarrier spacing, symbol duration and cyclic-prefix duration, respectively. OFDM signals are usually processed via a root raised-cosine (RRC) filter to reduce the inter-carrier interference. Let $w(t)$ define the RRC filter response, then an OFDM waveform consisting of L symbols over N_s subcarriers is given by [28]

$$u_{OFDM}(t) = \sum_{l=0}^{L-1} \sum_{n=-N_s/2}^{N_s/2-1} A s_{n,l} e^{j2\pi n \Delta f (t-T_{cp}-lT_{sym})} w(t - lT_{sym}). \tag{13}$$

The QAM symbols ($s_{n,l}$) transmitted in the waveform affect the power spectrum of the OFDM waveform over time, however, its overall bandwidth stays constant unlike FM signals. Therefore, DVB-T/DAB signals deliver a more reliable and finer range resolutions compared to FM signals in passive radar applications [7]. Since the power spectrum of OFDM signals are affected by the data transmitted, it is not possible to derive exact analytical FIM and CRLBs expressions. Therefore, modified FIM and CRLBs have been derived for OFDM signals [28]. Using Parseval's theorem and omitting the SNR, the first element of FIM is computed as [48]

$$[\mathbf{J}_0]_{1,1} = 4\pi^2 \int_{-\infty}^{+\infty} f^2 |U(f)|^2 \, df, \tag{14}$$

where $U(f)$ denotes the Fourier transform of $u(t)$. An approximate analytical expression of $\int_{-\infty}^{+\infty} f^2 |U(f)|^2 \, df$ for OFDM signals is given in [28], and substituting this in (14), the first element of the modified FIM for an OFDM waveform consisting of L OFDM symbols can be written as

$$[\mathbf{J}_{OFDM}]_{1,1} = \frac{4\pi^2 L \left(3 + \Delta f^2 \left(N_s^2 - 1\right)\left(4T_{sym} - T_w\right) T_w\right)}{\left(48T_{sym} - 12T_w\right) T_w}. \tag{15}$$

Moreover, the second element of FIM is given by [48]

$$[\mathbf{J}_0]_{2,2} = 4\pi^2 \int_{-\infty}^{+\infty} t^2 |u(t)|^2 \, dt, \tag{16}$$

and substituting the analytical expression of $\int_{-\infty}^{+\infty} t^2 |u(t)|^2 \, dt$ given by [28] for OFDM signals in (16), the last element of the modified FIM for an OFDM waveform consisting of L OFDM symbols can be given by (17). The other two elements of FIM for OFDM signals are given as $[\mathbf{J}_{OFDM}]_{1,2} = [\mathbf{J}_{OFDM}]_{2,1} = 0$ [28].

$$[\mathbf{J}_{OFDM}]_{2,2} = \frac{L\left[4\pi^2 L^2 T_{sym}^3 - \pi^2\left(L^2+2\right)T_{sym}^2 T_w - \left(\pi^2-6\right)T_w^3 + 12\left(\pi^2-8\right)T_{sym}T_w^2\right]}{12T_{sym} - 3T_w/4}. \tag{17}$$

4 Bistatic CRLBs on Range and Velocity Estimations

The bistatic geometry between Tx-target-Rx has a significant impact on range and velocity estimations, thus, the monostatic CRLBs are not valid in bistatic radar systems as demonstrated in the previous studies [5, 1, 40].Especially while the target is crossing or approaching to the baseline of the Tx-Rx pair, the forward scatter occurs and this substantially deteriorates the estimation of target parameters.

The bistatic CRLBs on range and velocity estimations were derived in [5] which also shows that bistatic CRLBs can be decoupled into geometry-related and waveform-related parameters. The bistatic FIM with regards to range R_i from target to receiver and target relative velocity $V_{i,j}$ to the receiver is given by [5]

$$\mathbf{J}\left(R_i, V_{i,j}\right) = -2\rho_{i,j}\begin{bmatrix} \frac{\partial^2\Theta(R_i,V_{i,j})}{\partial R_i^2} & \frac{\partial^2\Theta(R_i,V_{i,j})}{\partial R_i \partial V_{i,j}} \\ \frac{\partial^2\Theta(R_i,V_{i,j})}{\partial V_{i,j}\partial R_i} & \frac{\partial^2\Theta(R_i,V_{i,j})}{\partial V_{i,j}^2} \end{bmatrix}, \tag{18}$$

where partial derivatives of $\Theta\left(R_i, V_{i,j}\right)$ with respect to target range R_i and target relative velocity $V_{i,j}$ can be calculated as [5]

$$\begin{aligned}\frac{\partial^2\Theta\left(R_i,V_{i,j}\right)}{\partial R_i^2} &= \left[\mathbf{J}_0\right]_{1,1}\left(\frac{\partial\tau}{\partial R_i}\right)^2 \\ &\quad + 2\left[\mathbf{J}_0\right]_{1,2}\frac{\partial\tau}{\partial R_i}\frac{\partial\omega}{\partial R_i} + \left[\mathbf{J}_0\right]_{2,2}\left(\frac{\partial\omega}{\partial R_i}\right)^2,\end{aligned} \tag{19}$$

$$\frac{\partial^2\Theta\left(R_i,V_{i,j}\right)}{\partial V_{i,j}^2} = \left[\mathbf{J}_0\right]_{2,2}\left(\frac{\partial\omega}{\partial V_{i,j}}\right)^2, \tag{20}$$

$$\begin{aligned}\frac{\partial^2\Theta\left(R_i,V_{i,j}\right)}{\partial R_i\partial V_{i,j}} &= \frac{\partial^2\Theta\left(R_i,V_{i,j}\right)}{\partial V_{i,j}\partial R_i} \\ &= \left[\mathbf{J}_0\right]_{1,2}\frac{\partial\tau}{\partial R_i}\frac{\partial\omega}{\partial V_{i,j}} + \left[\mathbf{J}_0\right]_{2,2}\frac{\partial\omega}{\partial R_i}\frac{\partial\omega}{\partial V_{i,j}},\end{aligned} \tag{21}$$

where $\mathbf{J}_0$ denotes the FIM matrix resulting from only waveform related parameters as given for LFM, FM and OFDM waveforms in the previous section. This demonstrates that the bistatic CRLB of the selected Tx-Rx pairs can be decoupled into waveform and geometry related parameters, and this simplifies the calculations and reduces the computational complexity as waveform parameters are generally constant while the bistatic geometry varies over the time. To calculate the equations above, the analytical expressions of the partial derivations of geometry-related parameters are given by (23)-(28) [5]

$$\frac{\partial\omega}{\partial R_i} = \frac{f_c}{c_0}V_{i,j}\frac{L_{i,j}\cos^2\theta_i}{\left(R_i^2 + L_{i,j}^2 2R_iL_{i,j}\theta_i\right)^{3/2}\sqrt{\frac{1}{2}+\frac{R_i+L_{i,j}\sin\theta_i}{2\sqrt{R_i^2+L_{i,j}^2+2R_i\sin\theta_i}}}}, \tag{22}$$

$$\frac{\partial\omega}{\partial V_{i,j}} = \frac{2f_c}{c_0}\sqrt{\frac{1}{2}+\frac{R_i+L_{i,j}\sin\theta_i}{2\sqrt{R_i^2+L_{i,j}^2+2R_iL_{i,j}\sin\theta_i}}}, \tag{23}$$

$$\frac{\partial\tau}{\partial R_i} = \frac{1}{c_0}\left(1+\frac{R_{i.j}+L_{i,j}\sin\theta_i}{\sqrt{R_i^2+L_{i,j}^2+2R_i^2L_{i,j}\sin\theta_i}}\right), \tag{24}$$

$$\frac{\partial^2 \omega}{\partial R_i \partial V_{i,j}} = \frac{1}{V_{i,j}} \frac{\partial \omega}{\partial R_i}, \tag{25}$$

$$\frac{\partial^2 \tau}{\partial R_i^2} = \frac{L_{i,j}^2 \cos^2 \theta_i}{c_0 \left(R_i^2 + L_{i,j}^2 + 2R_i L_{i,j} \sin \theta_i\right)^{3/2}}, \tag{26}$$

$$\frac{\partial^2 \omega}{\partial R_i^2} = \frac{-\left[6\left(R_i^2 + L_{i,j}^2 + 2R_i L_{i,j} \sin \theta_i\right)^{1/2} \left(R_i + L_{i,j} \sin \theta_i\right) + \left(R_i^2 + L_{i,j}^2 + 2R_i L_{i,j} \sin \theta_i\right) + 5\left(R_i + L_{i,j} \sin \theta_i\right)^2\right]}{4c_0 \left(\sqrt{2} f_c V_{i,j} L_{i,j}^2 \cos^2 \theta_i\right)^{-1} \left(R_i^2 + L_{i,j}^2 + 2R_i L_{i,j} \sin \theta_i\right)^{9/4} \left[\left(R_i^2 + L_{i,j}^2 + 2R_i L_{i,j} \sin \theta_i\right)^{1/2} + \left(R_i + L_{i,j} \sin \theta_i\right)\right]^{3/2}}, \tag{27}$$

$$\frac{\partial \tau}{\partial V_{i,j}} = \frac{\partial^2 \tau}{\partial R_i \partial V_{i,j}} = \frac{\partial^2 \tau}{\partial V_{i,j}^2} = \frac{\partial^2 \omega}{\partial V_{i,j}^2} = 0, \tag{28}$$

where c_0 and f_c denote the speed of light and the carrier frequency, respectively.

5 Waveform and Tx-Rx Pair Selection

blueSubsequent to calculating CRLBs on the range and velocity for all Tx-Rx pairs for the entire area of interest, the best Tx-Rx pair for estimating the range or velocity of a target in a specific location can be selected depending on the CRLBs information. Consequently, the Tx-Rx pair providing the best range estimation (R_{pair}) can be selected by

$$blue R_{pair} = \underset{T_j R_i}{\operatorname{argmin}} \left(CRLB_{range}^{T_j R_i}\left(T_{loc}\right)\right), \tag{29}$$

blueand the best pair for the velocity estimation (V_{pair}) can be selected by

$$blue V_{pair} = \underset{T_j R_i}{\operatorname{argmin}} \left(CRLB_{velocity}^{T_j R_i}\left(T_{loc}\right)\right). \tag{30}$$

blueIn these equations, T_{loc} denotes the location of the target and $T_j R_i$ indicates the Tx-Rx pair consisting of the jth transmitter and the ith receiver while $CRLB_{range}^{T_j R_i}\left(T_{loc}\right)$ and $CRLB_{velocity}^{T_j R_i}\left(T_{loc}\right)$ denote the CRLBs on the range and velocity estimations of $T_j R_i$ pair at the T_{loc} locations. Note that the best velocity and range estimations might be achieved by different pairs, which is demonstrated in the next section.

6 Simulations and Numerical Results

In the simulated multistatic networks, four transmitters, i.e., active radar transmitter (LFM), DVB-T, DAB and FM radio broadcasting stations, and two multi-band receivers are placed in various locations in the area of interest, represented by a 3D coordinate system. For the sake of simplicity, only a single target is considered. The altitude of the target is 400 m, the height of FM, DVB-T, DAB transmitters and receiver antennas are considered as 100 m, 20 m, 20 m and 5 m, respectively. Other transmitter and waveform parameters used in the simulations are given in Table 1. Each Tx-Rx pair with the target creates a bistatic geometry of which CRLBs are computed in the simulations using the model explained in the previous sections. It should be noted that the target radar cross section (RCS) is assumed to be constant, i.e., 0 dBm^2 in each bistatic pair as we mainly focus on the impact of the bistatic geometry and waveforms. The DPI in passive bistatic pairs is assumed to be cancelled, hence, $\mu_{DPI} = 0$ in the simulations. The purpose of this analysis is to evaluate how the CRLB vary within a given defined scenario for four separate waveforms. This information could be used by an intelligent multistatic radar network to choose which waveforms to utilise in a tracking fusion engine.

An X-band radar transmitter emitting LFM waveform with 50 MHz bandwidth at 9.4 GHz carrier frequency is considered for the active radar operations. Since the antenna size is very small in X-band frequencies, an antenna array with a gain of 25 dBi at both transmitter and receiver are assumed for active sensing, resulting in 50 dBi total gain while

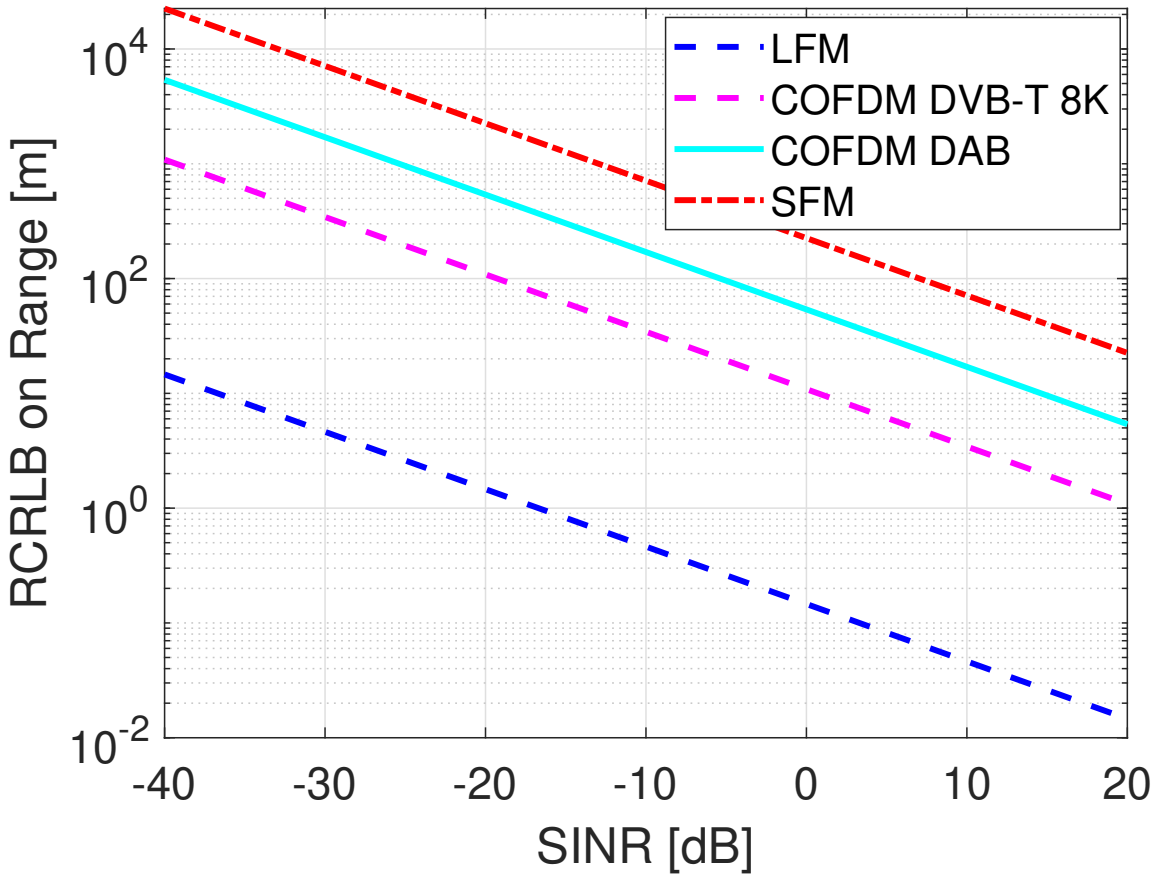

Figure 2: Monostatic RCRLB on range with different waveforms.

Table 1: Transmitter and waveform parameters

Waveform	Modulation	f_c	Bandwidth	Duration	Power	Antenna Gain
FM Radio	SFM	100 MHz	75 kHz	100 ms observation	20 kW	4.3 dBi
DVB-T 8K	COFDM	500 MHz	7.61 MHz	64 symbols in 57.3 ms	5 kW	4.3 dBi
DAB	COFDM	150 MHz	1.536 MHz	64 symbols in 40 ms	5 kW	4.3 dBi
Radar Chirp	LFM	9.4 GHz	50 MHz	64 pulses in 25.6 ms	10 kW	50 dBi

dipole antennas with a gain of 2.15 dBi at both ends are considered for broadcasting signals to provide an omnidirectional coverage. An LFM waveform consisting of 64 pulses with $T_p = 200$ μs pulse duration and $T_r = 400$ μs pulse repetition interval are considered for active sensing while 100 ms signal observation is used for passive sensing with FM signals and 64 OFDM symbols are utilised for DVB-T and DAB signals.

Monostatic root CRLBs (RCRLBs) on range and velocity estimations as a function of SNR for FM radio, DVB-T, DAB and LFM waveforms are presented in Fig. 2 and Fig. 3, respectively. It is observed that the LFM waveform substantially outperforms others in terms of range estimation due to its wider bandwidth, however, the gap between RCRLB on velocity estimations are narrower since velocity estimation is mainly related to the observation time.

Fig. 4 illustrates the first scenario considered for the multistatic radar network, where a single target moves forward along the x-axis starting from 0 km position. It is worth noting that Tx1 and Rx1 are close to each other, thus, they create a quasi monostatic active radar system, and Rx2 is placed at (0,0) location. The SINR of the signals at receivers of scenario 1 is presented in Fig. 5 while the targets moves along the x-axis. Due to the very high carrier frequency, i.e., 9.4 GHz, the SINR of the active radar is lower, especially compared to FM radio signals which have the lowest carrier frequency, hence, encounters a lower path-loss. The bistatic RCRLBs on range and velocity estimations of this

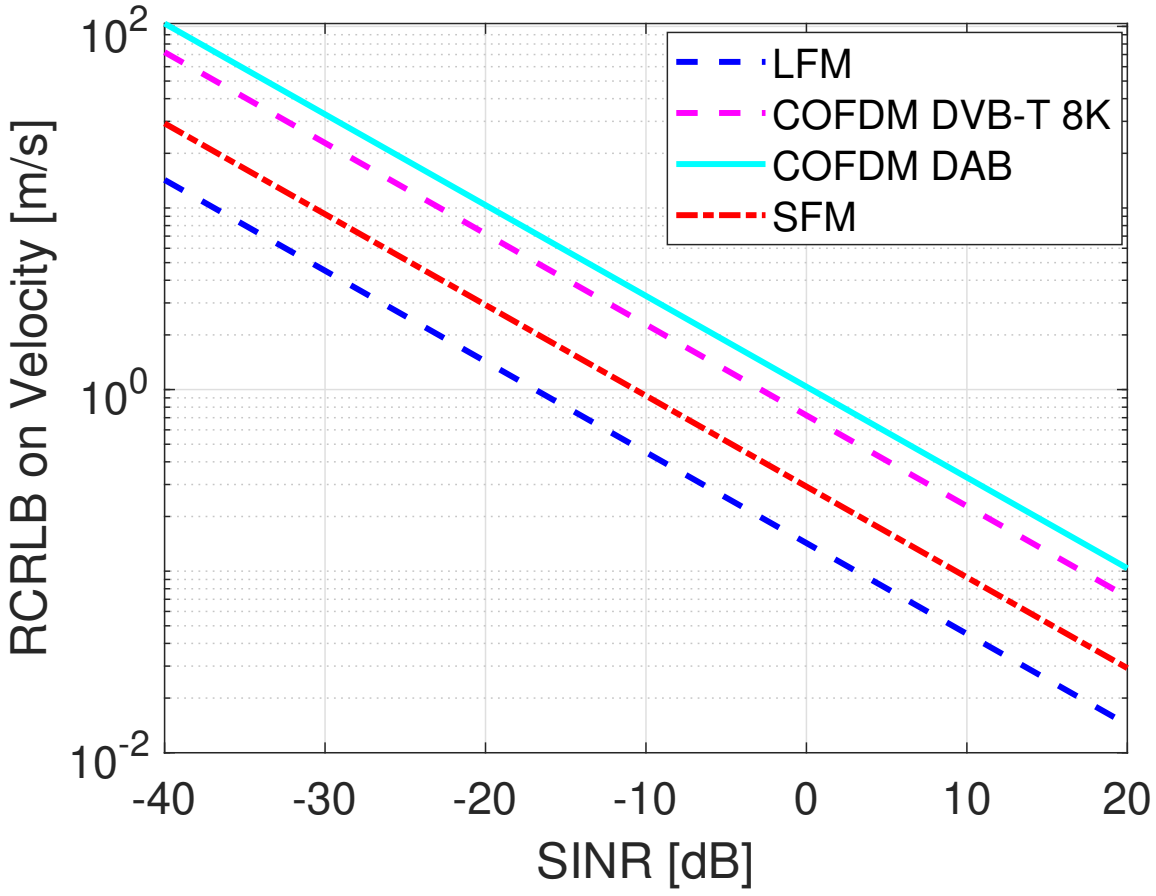

Figure 3: Monostatic RCRLB on velocity with different waveforms.

scenario are given by Fig. 6 and Fig. 7, respectively. Taking into account the bistatic geometries between the Tx-Rx pairs presented in Fig. 4, the impact of the bistatic geometry is clearly observed in Fig. 6 and Fig. 7 such that RCRLBs rapidly increase when the target approaching or crossing the baseline of the Tx-Rx pairs, resulting higher range and velocity estimation errors. Therefore, as the target moves forward, different Tx-Rx pairs become more desirable for estimating the target parameters. For instance, when the target is at around 10 km x-position, the DVB-T transmitter provides a better range and velocity estimations for a short time than the active radar transmitter. When the target is far away, FM signals may provide more accurate velocity estimations as shown in Fig. 7. On the other hand, in the case of jamming active radar transmitter, passive sensing may still provide a reasonable target parameter estimations as they would probably not be affected by jamming. Therefore, intelligently selecting Tx-Rx pairs are important to achieve the best estimation accuracies in the entire multistatic radar network.

In the second scenario illustrated in Fig. 8, Rx2 is placed at (40,3) km location and it is considered that the target follows a diagonal trajectory and crosses the baseline of different Tx-Rx pairs over time. Similar to Scenario 1, the SINR of the received signals at the receivers vary over time as the target moves forward, as shown in Fig. 9. The change of the RCRLBs with regard to bistatic geometry is also observed in this scenario as the target crosses baseline of Tx-Rx pairs while moving. For example, although the SINR of Tx3-Rx1 pair increase as the target moves, a significant peak in the RCRLBs of this pair is also observed at the same time since the target approaches the baseline of this pair. Fig. 10 indicates that Tx2-Rx1 (DVB-T) and Tx4-Rx2 (DAB) pairs may provide sufficient range estimations in different parts of the target trajectory since they achieve the lowest RCRLBs on range after the active radar pairs. However, it is important to select correct Tx-Rx pairs for the different parts of the target trajectory. For instance, when the target is around 50 km x-position, Tx3-Rx2 (FM) may achieve the best range estimation for a short time owing to its very high SINR value at this point. A similar situation can also be observed in the case of velocity estimation as shown in Fig. 11. These results show that an active radar transmitter can be supported by passive radar sensing opportunities to improve the accuracy of range and velocity estimations and even it may be possible to avoid jamming

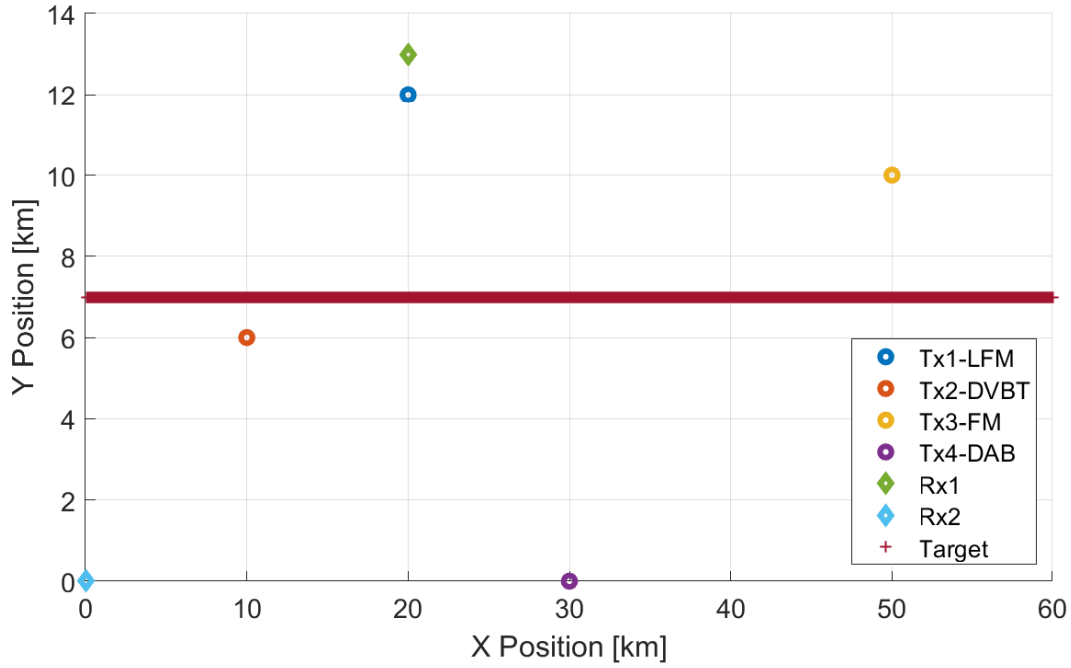

Figure 4: Scenario 1.

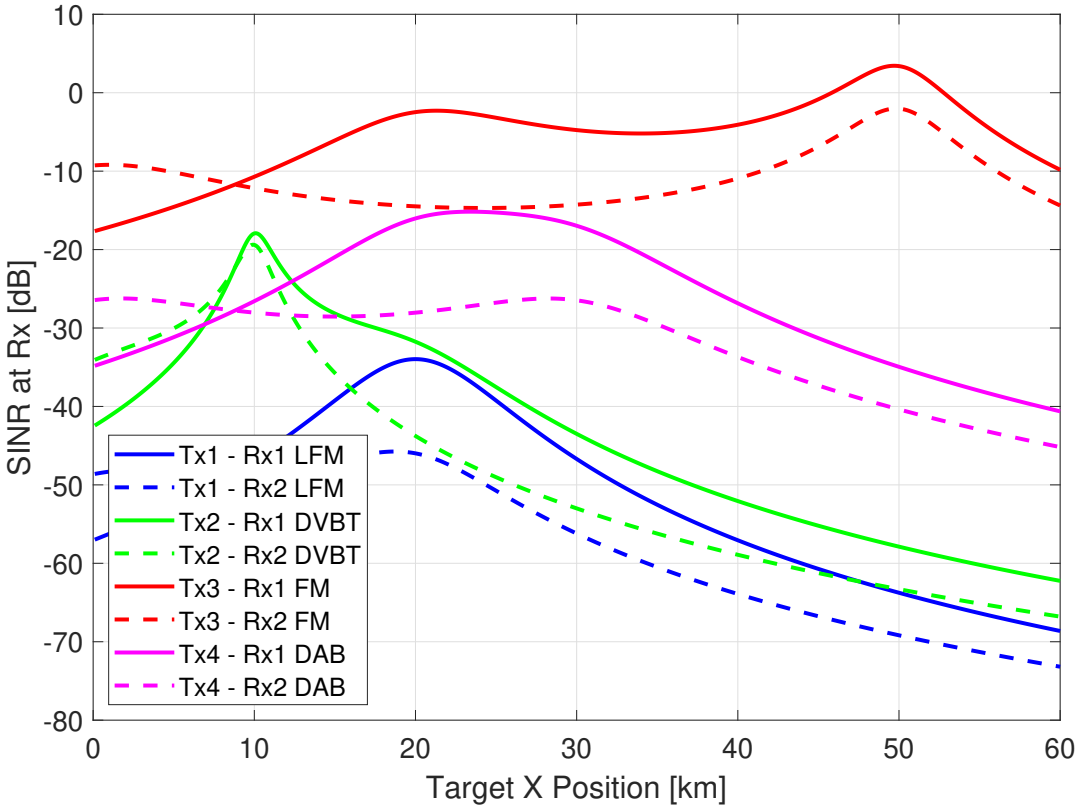

Figure 5: SINR of scenario 1.

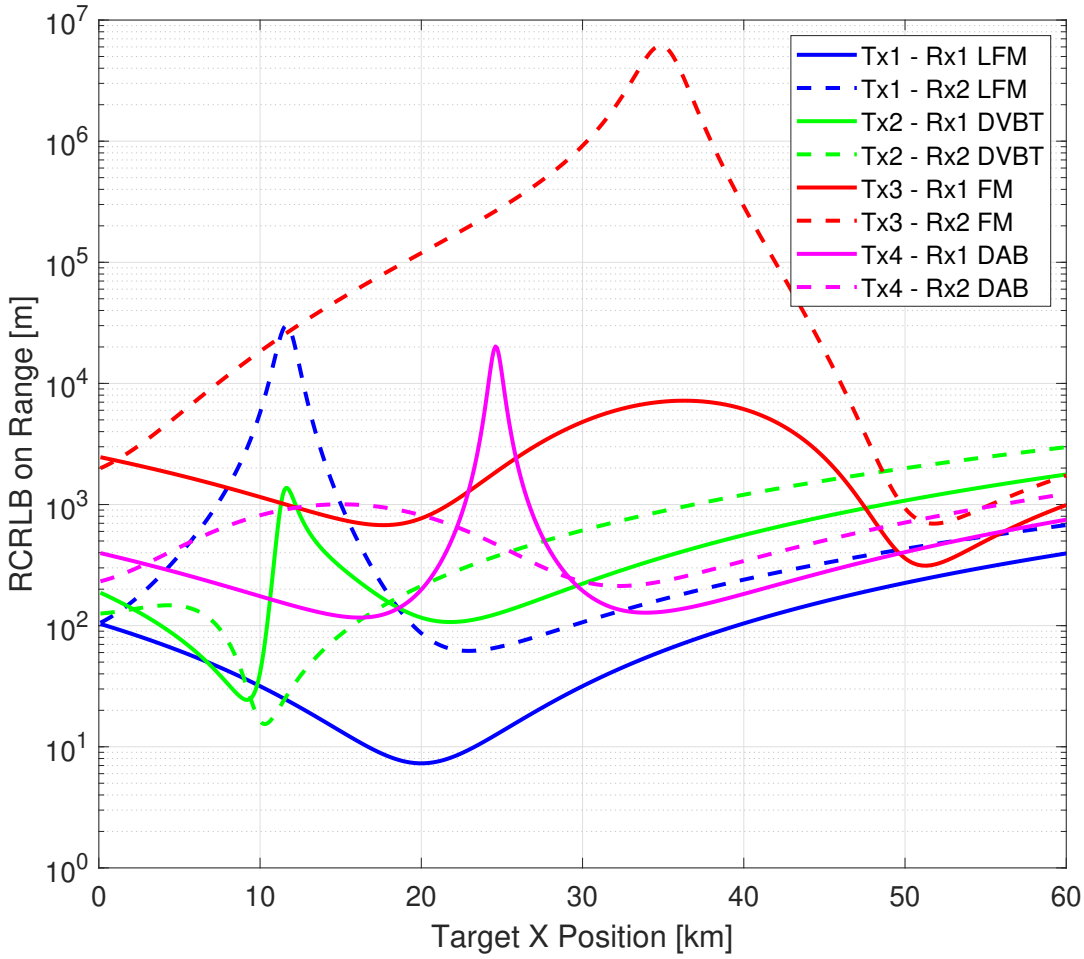

Figure 6: RCRLB on range in scenario 1.

or to switch off the active transmitter for certain times where passive bistatic sensing may provide sufficiently accurate estimations.

Fig. 12 and Fig. 13 present the average RCRLBs on range and velocity of all pairs and also combination of all of them and combination of only passive sensing pairs in the scenarios considered and explained above. Combination of all pairs is obtained by selecting the pairs which deliver the best estimation accuracy for a given target location. It should be noted that the maximum RCRLBs are limited to 10^3 for both range and velocity estimations while calculating the average RCRLBs presented in these figures to reduce the impact of the outliers on the averages. It can be seen that active monostatic pair provides the best average estimation in both scenarios since other Tx-Rx pairs encounter forward scatter which deteriorates the estimations, hence increases the average RCRLBs. However, in some target locations, one or two passive sensing pairs may provide better estimation than active sensing as a result of high SINR obtained from these pairs or bistatic active sensing might be degraded by the bistatic geometry. Therefore, selecting the pairs providing the best estimations improves the overall estimation accuracy of the multistatic network. For instance, in scenario 1 presented in Fig. 12, selecting the best Tx-Rx pairs significantly improves the average velocity estimations. Moreover, in scenario 2 presented in Fig. 13, this optimum Tx-Rx pair selection significantly improves both range and velocity estimations compared to using only active quasi-monostatic (Tx1-Rx1) pair.

While average expected estimation errors are relatively high for each passive sensing pair, however, by combining only passive pairs provided reasonable RCRLBs in both scenarios as indicated by 'Combined-Passive' in Fig. 12 and Fig. 13. This demonstrates the importance of having multi-band multi-waveform receivers and utilising two or more IOs in the area of interest to achieve a desirable target parameter estimation accuracy. Based on the information

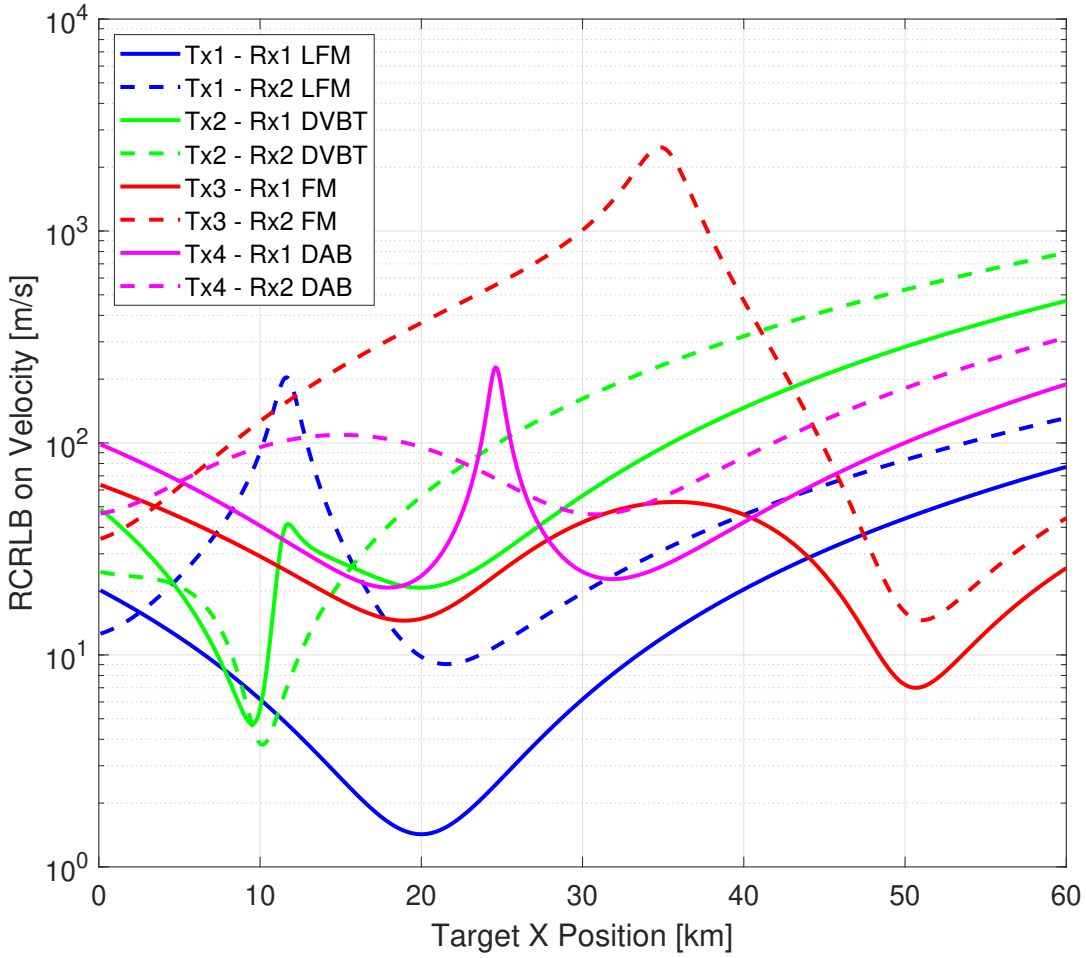

Figure 7: RCRLB on velocity in scenario 1.

obtained from these simulations, the radar can switch between the waveforms and even can switch off emitting LFM waveform to perform in entirely passive mode when it is necessary depending on the target location. Moreover, in the case of jamming, the radar can decide using another waveform which is not jammed since the carrier frequencies of the waveforms are significantly different. The impact of simple jamming on CRLBs is modeled as an extra interference on the received signal [49], therefore, jamming degrades the SINR of the received radar returns, hence, degrades range and velocity estimations performed through the active radar Tx-Rx pairs since jamming mainly targets the active radar waveform.

To further investigate the benefits of multistatic passive sensing, we have further evaluated the RCRLBs of the multistatic passive radar networks considered in the aforementioned two scenarios. In this analysis, Tx1 (active radar transmitter) is switched off and the RCRLBs on range and velocity estimations of the entire area of interest via passive multistatic radar networks consisting of three broadcasting stations and two receivers are computed. The resolution of this computation is 1 km such that the entire area of interest is divided into 1×1 km observation areas. As the central processor of the multistatic radar network knows the location of broadcasting stations, it can select the best Tx-Rx pair for a given 1×1 km observation area. By doing so, the minimum RCRLBs of the entire area of interest are computed. The minimum RCRLBs on the range and velocity estimations of the entire area of interest are presented in Fig. 14 and Fig. 15 for scenario 1, and in Fig. 16 and Fig. 17 for scenario 2. In other words, these figures present the theoretically lowest range and velocity estimation errors of the multistatic passive radar network which utilises only broadcasting signals and intelligently selects the best Tx-Rx pairs for any given location of the area surveillanced. The location of the transmitters and receivers are also shown in these figures to reveal how the estimation errors vary with regard to the

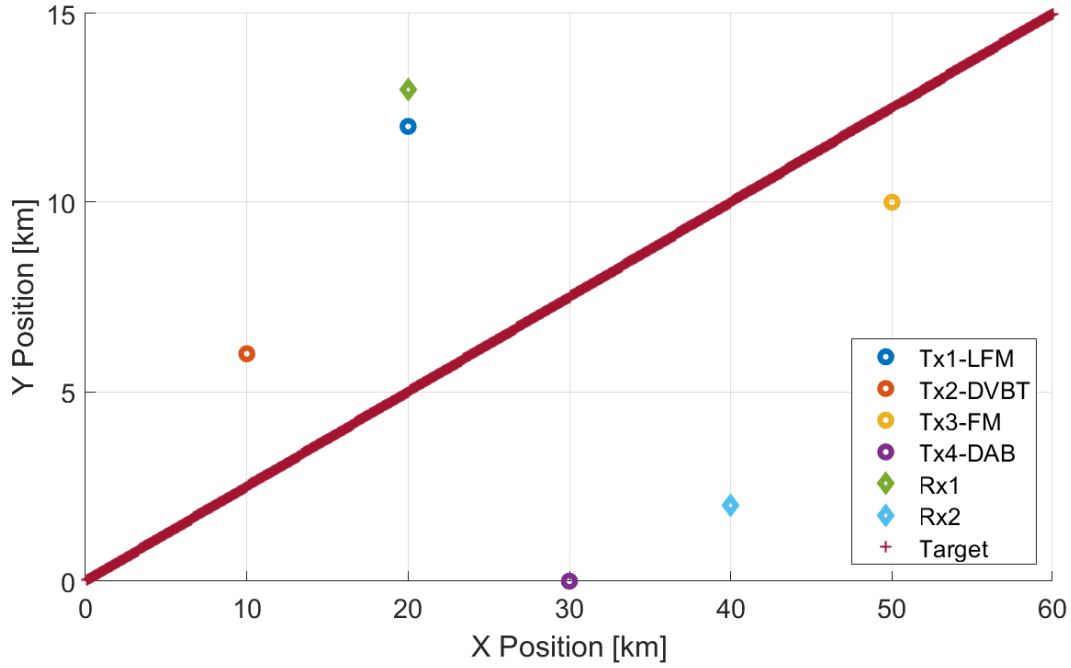

Figure 8: Scenario 2.

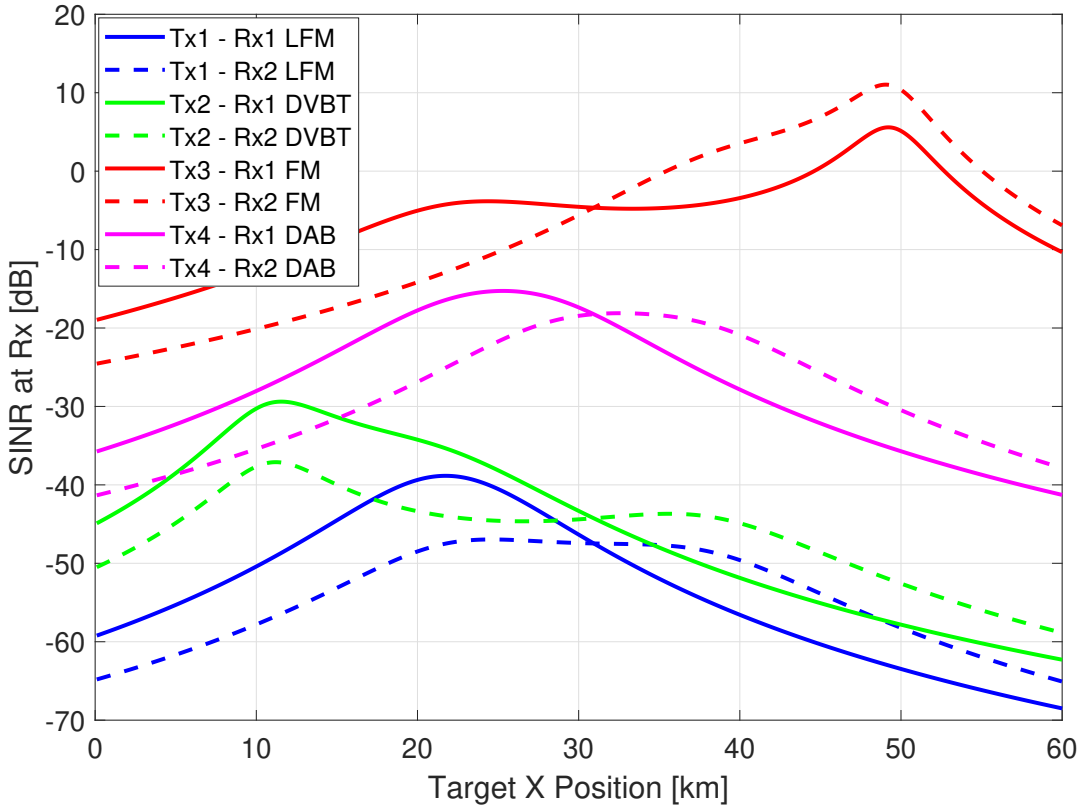

Figure 9: SINR of scenario 2.

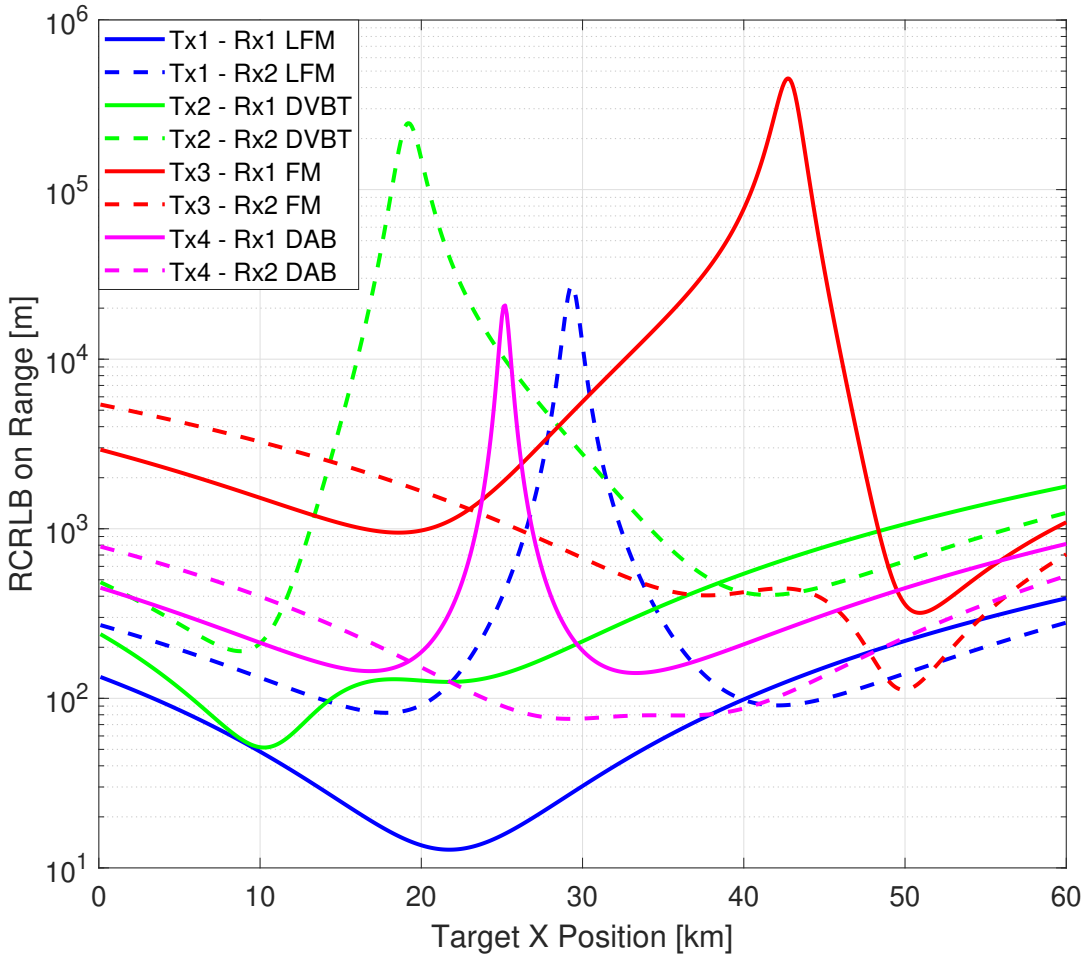

Figure 10: RCRLB on range in scenario 2.

transmitter and receiver locations. The only difference between scenario 1 and scenarios 2 is that Rx2 is moved from (0,0) to (40,3) km location in the scenario 2. It is observed that changing its location has significantly improved the overall range and velocity estimations since Rx2 has become closer to Tx3 (FM) and Tx4 (DAB) and the multistatic radar network has had more uniform Tx-Rx distribution over the area.

Comparing the range estimations of the two networks presented in Fig. 14 and Fig. 16, it is observed that the scenario 2 has a wider coverage with lower range estimation errors because of more efficiently utilising Tx3 (FM) and Tx4 (DAB) transmitters. These two figures also reveal that Tx2 (DVBT) and Tx4 (DAB) transmitters contribute to the range estimation significantly more than Tx3 (FM) as expected since the RCRLBs on range estimations around these transmitters are lower because of wider bandwidths of DVB-T and DAB signals compared to FM radio signals. In terms of velocity estimations, Tx3 (FM) transmitter can also be efficiently utilised as observed in Fig. 15 and Fig. 17 since velocity estimation is mainly related to the observation time of the radar returns. The impact of the bistatic geometry has been clearly observed on the left side of the Tx3 (FM) in Fig. 15, where higher velocity estimation errors are observed (indicated by blue and pink colours) since both Rx1 and Rx2 are placed on the left of Tx3 (FM). Therefore, the baselines of Tx3-Rx1 and Tx3-Rx2 are close to each other in this region where this leads to higher velocity estimation errors for both receivers due to the bistatic geometry of both Tx-Rx pairs. On the other hand, this situation does not occur in scenario 2 presented in Fig. 17 since the new location of Rx2 enables it to cover that blind area by changing its baseline with Tx3 (FM) to another direction. However, in Fig. 17, an area with a slightly lower velocity estimation accuracy (indicated by green colour between Tx3-Rx2) is observed between Tx3-Rx2 due to the bistatic geometry although it is still much more accurate than the situation observed in scenario 1.

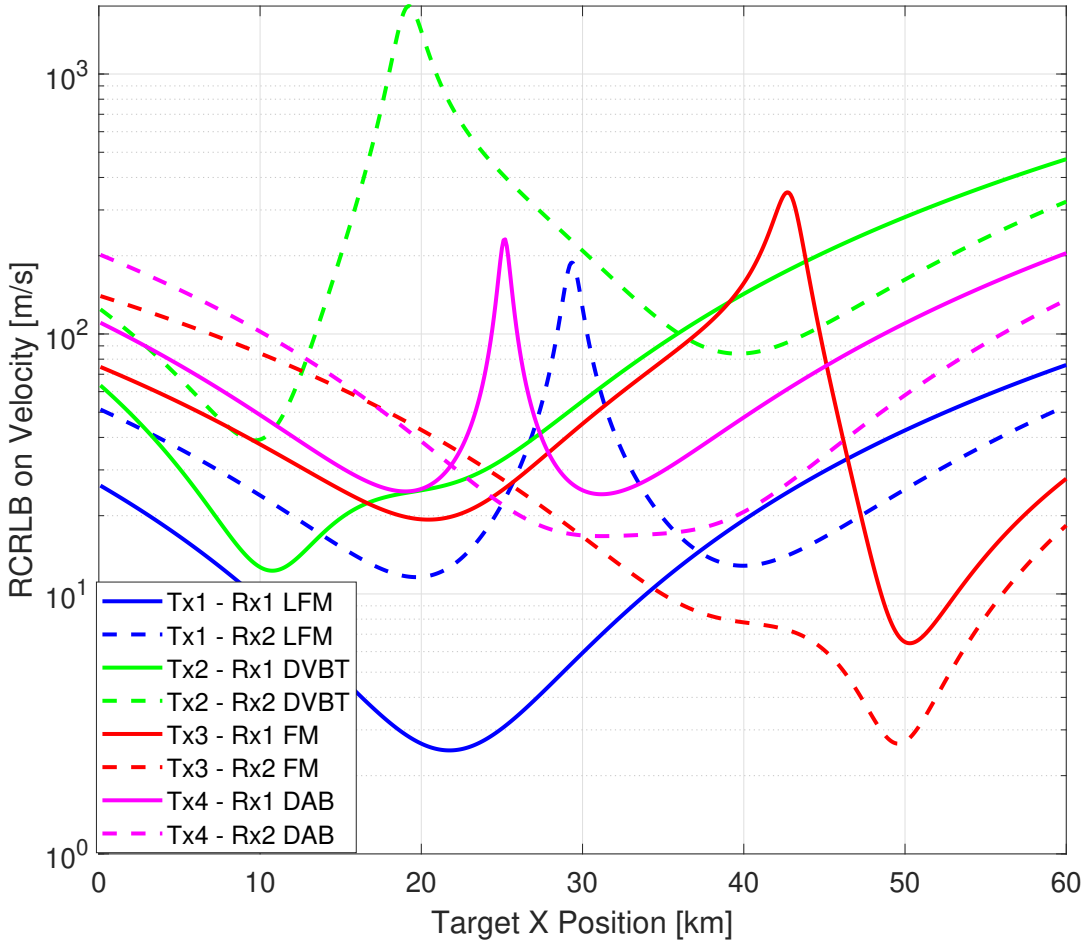

Figure 11: RCRLB on velocity in scenario 2.

Fig. 14, Fig. 15, Fig. 16 and Fig. 17 demonstrate that the range and velocity estimation accuracies are generally better around the transmitters and receivers unless the forward scatter occurs. Nevertheless, utilising multiple IOs as transmitters and intelligently placing the receivers can alleviate the impact of the forward scatter, hence, can improve the overall estimation performance as seen in the comparison of these two scenarios. Overall passive sensing estimation accuracy of the radar network presented in scenario 2 is better than the other one presented in scenario 1 and this is also seen in the comparisons of average RCRLBs on range and velocity estimations presented in Fig. 12 and Fig. 13. Another important observation is that the accuracy of velocity estimation is generally better than the accuracy of range estimation in the passive radar networks considered here since the bandwidth of the FM radio signals is too narrow to provide a sufficient range estimation accuracy, but it covers a wide area and provides an acceptable velocity estimation accuracy with a reasonably selected observation time.

This modelling and analysis can be performed for a real multi-band multistatic radar network scenario since the locations of broadcasting stations are fixed and known, and the locations of active radar transmitter and receivers are known by the radar. Based on this information, the radar system will be able to create a lookup table which contains the information of the best pairs for the different locations in the area of interest for passive sensing, therefore, the radar can choose the best Tx-Rx pairs which provide the lowest CRLBs to obtain the best possible range and velocity information of the target.

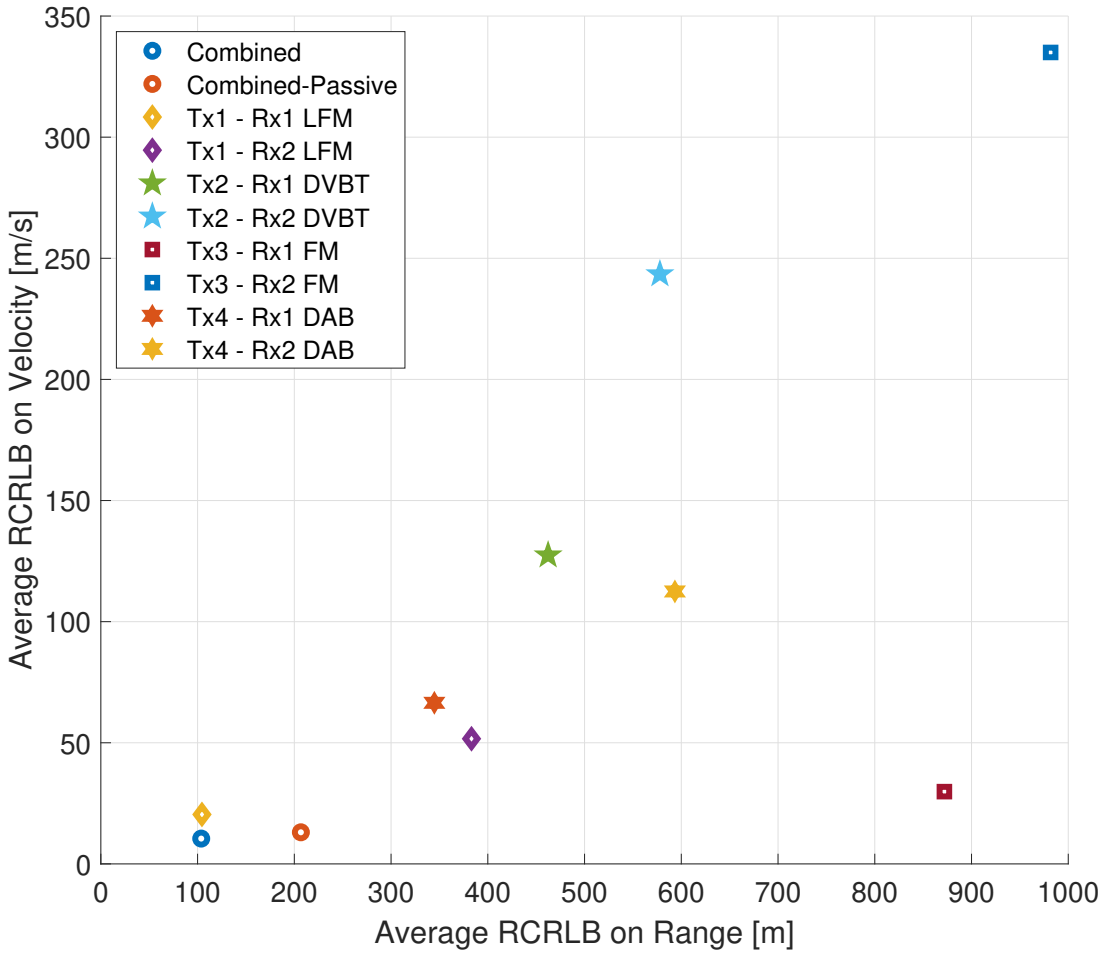

Figure 12: Average RCRLBs on velocity and range in scenario 1.

7 Conclusion

In this study, we have investigated multi-band multistatic radar networks which utilise an active radar transmitter and also IOs such as DVB-T, DAB and FM radio signals for providing improved velocity and range estimations. As a performance metric, the bistatic CRLBs of Tx-Rx pairs are used, which determine theoretical lower bounds of estimation errors. The results have demonstrated that bistatic geometry significantly impacts range and velocity estimations, therefore, relying on only a single transmitter may result in some blind areas in the radar network, especially around the baseline of the Tx-Rx pair. Moreover, the results shown would vary with new geometries, however, the importance shown here is that different waveforms can provide better estimations at different points of a scenario. Knowledge of this is very important for future cognitive/intelligent radar systems which may be looking to decide what signal to use to perform their sensing. Currently radar systems typically only use their own waveform which is represented by the case of the Tx1-Rx1 LFM co-located pair in this study. The analysis shown here gives an insight into the potential advantages of considering other IOs available in the area of interest in addition to active sensing pairs. A fused multi-band multistatic sensing system brings significant benefits and also provides a robustness to any possible jamming which is generally designed to corrupt active radar waveform, hence, active sensing Tx-Rx pairs. Consequently, radar fusion systems should be the future direction of intelligent RF sensor networks.

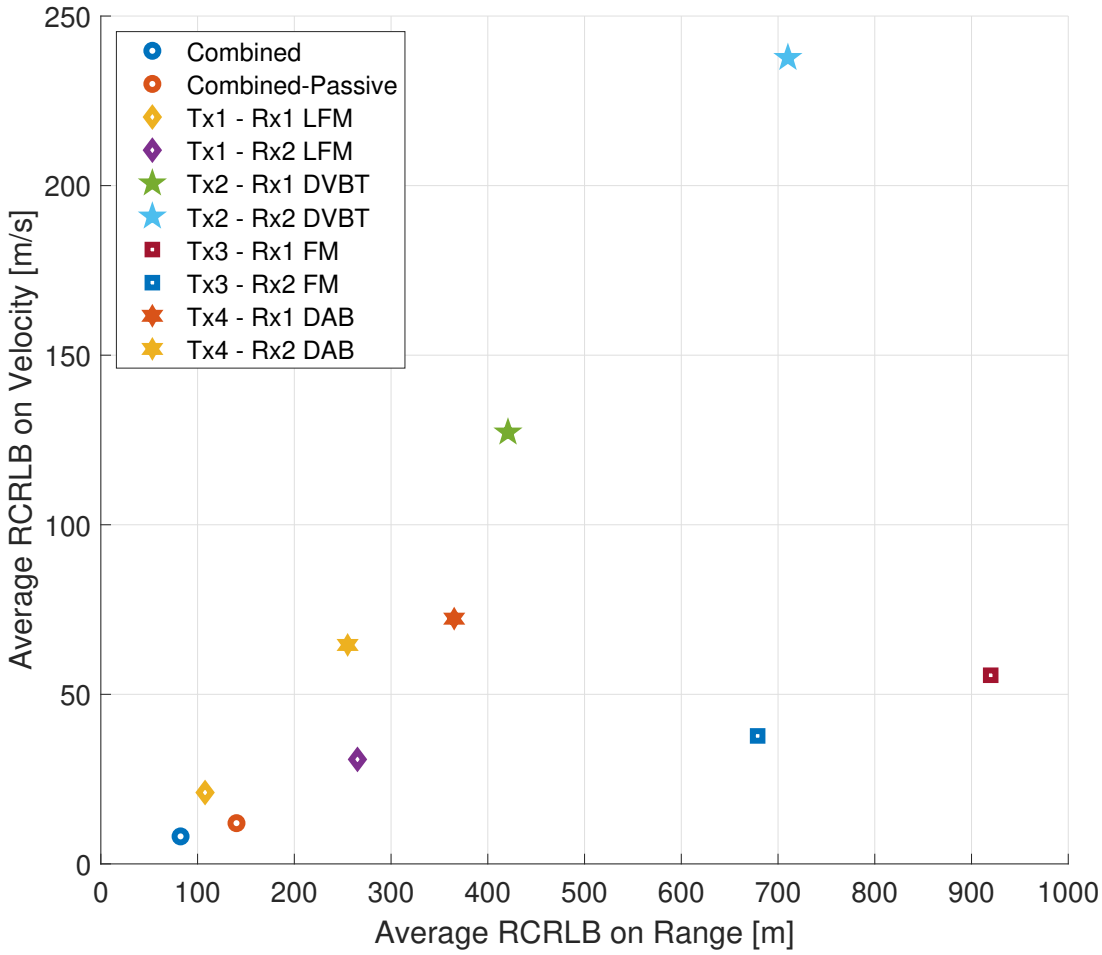

Figure 13: Average RCRLBs on velocity and range in scenario 2.

References

[1] H. D. Griffiths and C. J. Baker, *An introduction to passive radar*. Artech House, 2017.

[2] H. Kuschel, D. Cristallini, and K. E. Olsen, "Tutorial: Passive radar tutorial," *IEEE Aerospace and Electronic Systems Magazine*, vol. 34, pp. 2–19, Feb 2019.

[3] M. S. Greco, F. Gini, P. Stinco, and K. Bell, "Cognitive radars: On the road to reality: Progress thus far and possibilities for the future," *IEEE Signal Processing Magazine*, vol. 35, pp. 112–125, July 2018.

[4] P. Stinco, M. Greco, F. Gini, and M. Rangaswamy, "Ambiguity function and Cramér–Rao bounds for universal mobile telecommunications system-based passive coherent location systems," *IET Radar, Sonar & Navigation*, vol. 6, no. 7, pp. 668–678, 2012.

[5] M. S. Greco, P. Stinco, F. Gini, and A. Farina, "Cramer-Rao bounds and selection of bistatic channels for multistatic radar systems," *IEEE Transactions on Aerospace and Electronic Systems*, vol. 47, pp. 2934–2948, October 2011.

[6] A. S. Evers, *Evaluation and application of LTE, DVB, and DAB signals of opportunity for passive bistatic SAR imaging*. PhD thesis, Wright State University, 2014.

[7] S. Paine, F. Schonken, M. Malape, D. W. O'Hagan, J. Swart, F. Louw, and M. Setsubi, "Multi band FM and DVB-T2 passive radar demonstrator," in *2018 19th International Radar Symposium (IRS)*, pp. 1–10, June 2018.

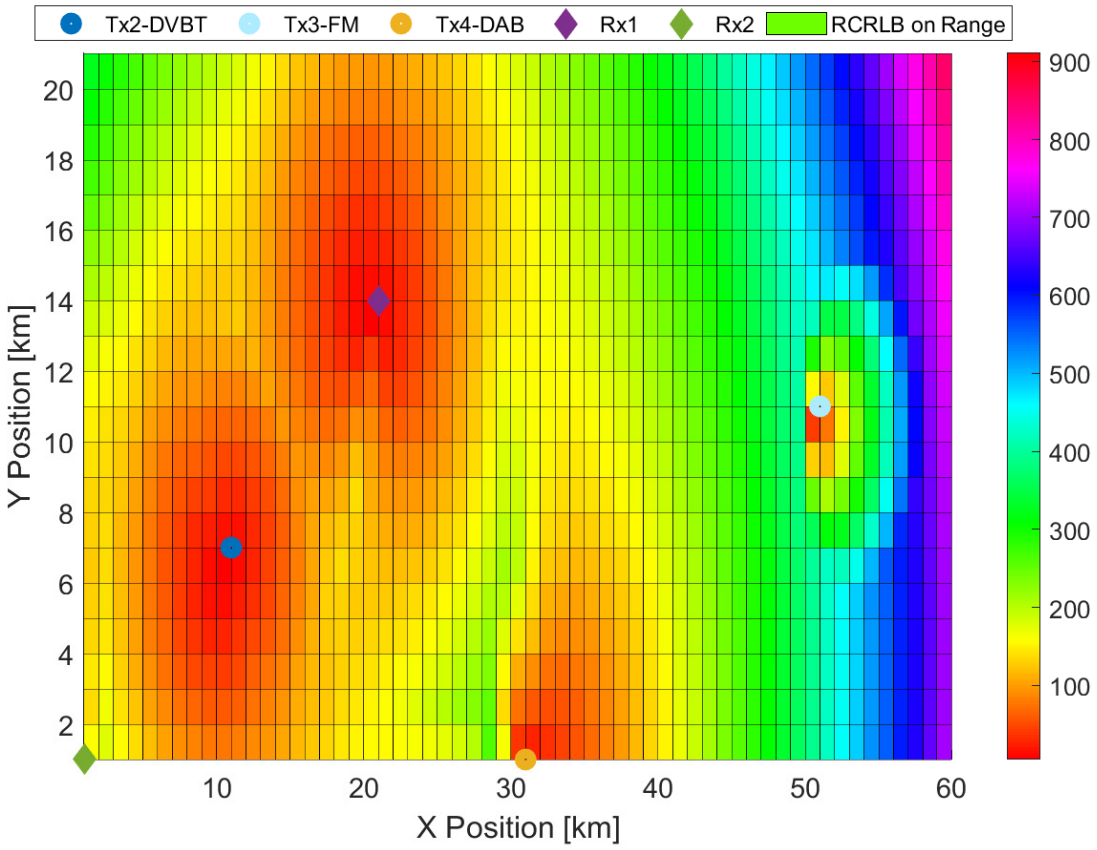

Figure 14: Minimum RCRLBs on range of the area of interest surveillanced by multistatic passive radar system in scenario 1.

[8] M. Edrich, A. Schroeder, and F. Meyer, "Design and performance evaluation of a mature FM/DAB/DVB-T multi-illuminator passive radar system," *IET Radar, Sonar & Navigation*, vol. 8, no. 2, pp. 114–122, 2014.

[9] C. Shi, F. Wang, M. Sellathurai, and J. Zhou, "Transmitter subset selection in FM-based passive radar networks for joint target parameter estimation," *IEEE Sensors Journal*, vol. 16, pp. 6043–6052, Aug 2016.

[10] B. Dawidowicz, P. Samczynski, M. Malanowski, J. Misiurewicz, and K. S. Kulpa, "Detection of moving targets with multichannel airborne passive radar," *IEEE Aerospace and Electronic Systems Magazine*, vol. 27, pp. 42–49, November 2012.

[11] K. Chetty, G. E. Smith, and K. Woodbridge, "Through-the-wall sensing of personnel using passive bistatic WiFi radar at standoff distances," *IEEE Transactions on Geoscience and Remote Sensing*, vol. 50, pp. 1218–1226, April 2012.

[12] Y. Zhou, B. P. L. Lau, Z. Koh, C. Yuen, and B. K. K. Ng, "Understanding crowd behaviors in a social event by passive WiFi sensing and data mining," *IEEE Internet of Things Journal*, vol. 7, pp. 4442–4454, May 2020.

[13] Z. Geng, R. Xu, and H. Deng, "LTE-based multistatic passive radar system for UAV detection," *IET Radar, Sonar & Navigation*, vol. 14, no. 7, pp. 1088–1097, 2020.

[14] O. Mahfoudia, F. Horlin, and X. Neyt, "Performance analysis of the reference signal reconstruction for DVB-T passive radars," *Signal Processing*, vol. 158, pp. 26–35, 2019.

[15] O. Mahfoudia, F. Horlin, and X. Neyt, "Optimum reference signal reconstruction for DVB-T based passive radars," in *2017 IEEE Radar Conference (RadarConf)*, pp. 1327–1331, IEEE, 2017.

[16] Q. Chen, X. Zhang, Q. Yang, L. Ye, and M. Zhao, "Performance bound for joint multiple parameter target estimation in sparse stepped-frequency radar: A comparison analysis," *Sensors*, vol. 19, no. 9, 2019.

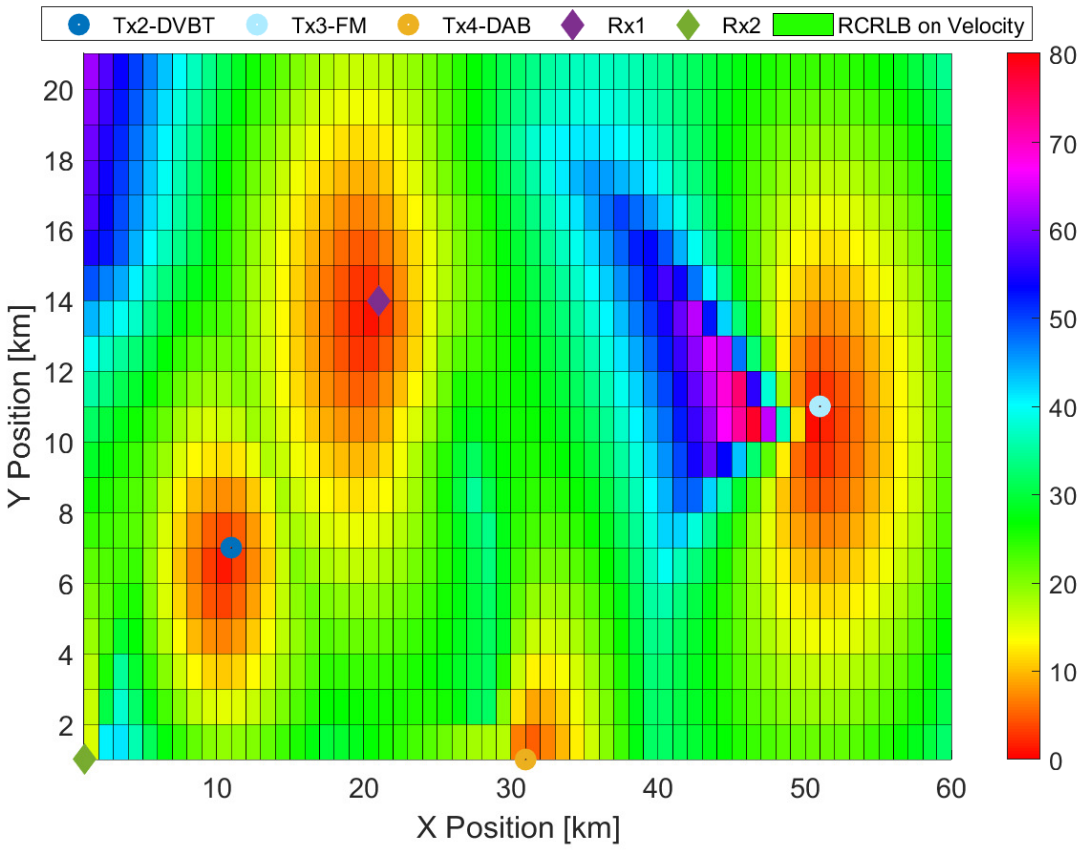

Figure 15: Minimum RCRLBs on velocity of the area of interest surveillanced by multistatic passive radar system in scenario 1.

[17] P. You, Z. Ding, L. Qian, M. Li, X. Zhou, W. Liu, and S. Liu, "A motion parameter estimation method for radar maneuvering target in gaussian clutter," *IEEE Transactions on Signal Processing*, vol. 67, no. 20, pp. 5433–5446, 2019.

[18] H. Godrich, A. M. Haimovich, and R. S. Blum, "Target localization accuracy gain in MIMO radar-based systems," *IEEE Transactions on Information Theory*, vol. 56, pp. 2783–2803, June 2010.

[19] L. Gaudio, M. Kobayashi, G. Caire, and G. Colavolpe, "On the effectiveness of OTFS for joint radar parameter estimation and communication," *IEEE Transactions on Wireless Communications*, vol. 19, pp. 5951–5965, Sep. 2020.

[20] F. Zhang, Z. Zhang, W. Yu, and T.-K. Truong, "Joint range and velocity estimation with intrapulse and intersubcarrier doppler effects for OFDM-based RadCom systems," *IEEE Transactions on Signal Processing*, vol. 68, pp. 662–675, 2020.

[21] Y. Liu, G. Liao, Y. Chen, J. Xu, and Y. Yin, "Super-resolution range and velocity estimations with OFDM integrated radar and communications waveform," *IEEE Transactions on Vehicular Technology*, vol. 69, pp. 11659–11672, Oct 2020.

[22] F. Zhang, Y. Sun, J. Zou, D. Zhang, and Q. Wan, "Closed-form localization method for moving target in passive multistatic radar network," *IEEE Sensors Journal*, vol. 20, pp. 980–990, Jan 2020.

[23] H. Zhang, B. Zong, and J. Xie, "Power and bandwidth allocation for multi-target tracking in collocated MIMO radar," *IEEE Transactions on Vehicular Technology*, vol. 69, pp. 9795–9806, Sep. 2020.

[24] V. M. Chiriac, Q. He, A. M. Haimovich, and R. S. Blum, "Ziv–Zakai bound for joint parameter estimation in mimo radar systems," *IEEE Transactions on Signal Processing*, vol. 63, pp. 4956–4968, Sep. 2015.

[25] A. Dogandzic and A. Nehorai, "Cramer-Rao bounds for estimating range, velocity, and direction with an active array," *IEEE Transactions on Signal Processing*, vol. 49, pp. 1122–1137, June 2001.

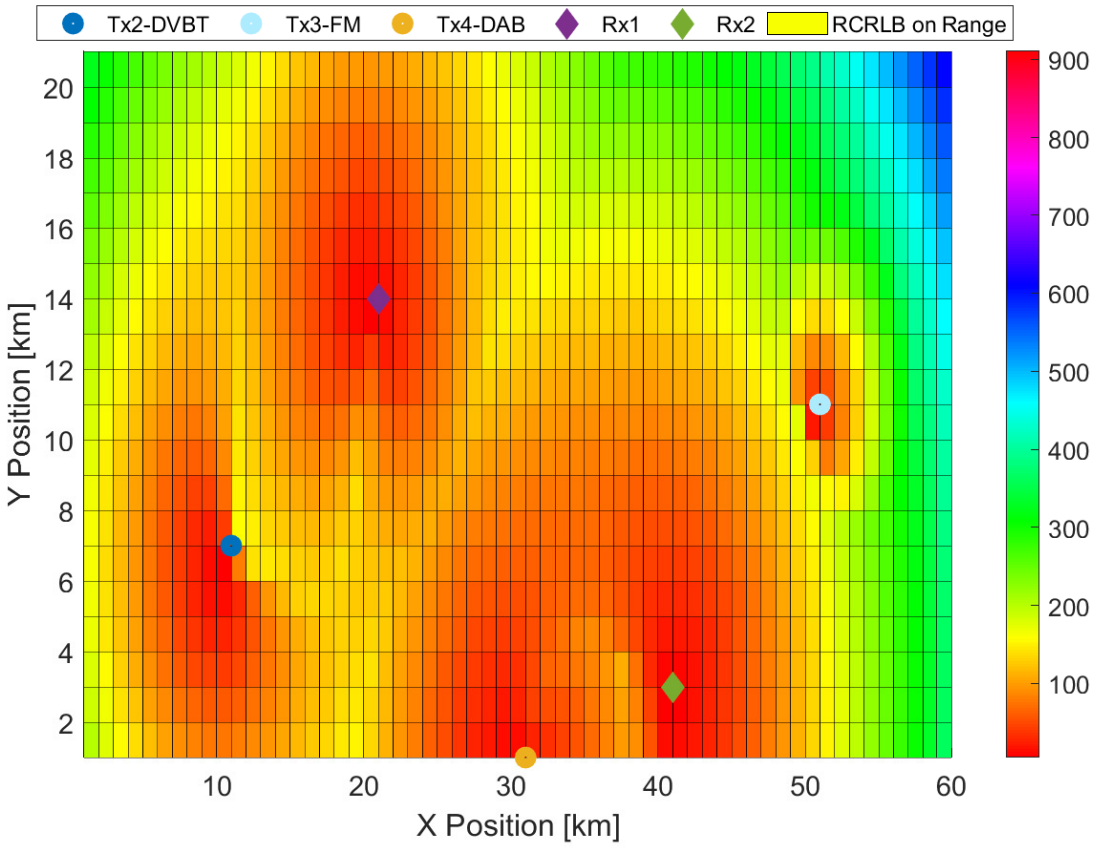

Figure 16: Minimum RCRLBs on range of the area of interest surveillanced by multistatic passive radar system in scenario 2.

[26] C. G. Shi, F. Wang, S. Salous, and J. J. Zhou, "Cramér-Rao lower bounds for joint target parameter estimation in FM-Based distributed passive radar network with antenna arrays," *Radio Science*, vol. 53, no. 3, pp. 314–333, 2018.

[27] C. G. Shi, S. Salous, F. Wang, and J. J. Zhou, "Modified Cramér-Rao lower bounds for joint position and velocity estimation of a rician target in OFDM-based passive radar networks," *Radio Science*, vol. 52, pp. 15–33, Jan 2017.

[28] A. Filip and D. Shutin, "Cramér–Rao bounds for L-band digital aeronautical communication system type 1 based passive multiple-input multiple-output radar," *IET Radar, Sonar & Navigation*, vol. 10, no. 2, pp. 348–358, 2016.

[29] M. A. Alslaimy, R. J. Burkholder, and G. E. Smith, "Measurements accuracy evaluation for ATSC signal based passive radar systems," *IEEE Transactions on Aerospace and Electronic Systems*, pp. 1–1, 2021.

[30] S. Gogineni, M. Rangaswamy, B. D. Rigling, and A. Nehorai, "Cramér-Rao bounds for UMTS-Based passive multistatic radar," *IEEE Transactions on Signal Processing*, vol. 62, pp. 95–106, Jan 2014.

[31] M. Rashid and M. Naraghi-Pour, "Multitarget joint delay and Doppler-shift estimation in bistatic passive radar," *IEEE Transactions on Aerospace and Electronic Systems*, vol. 56, pp. 1795–1806, June 2020.

[32] F. Liu, Y.-F. Liu, A. Li, C. Masouros, and Y. C. Eldar, "Cramér-Rao bound optimization for joint radar-communication beamforming," *IEEE Transactions on Signal Processing*, vol. 70, pp. 240–253, 2022.

[33] M. Greco, P. Stinco, F. Gini, A. Farina, and M. Rangaswamy, "Cramér-Rao bounds and Tx-Rx selection in a multistatic radar scenario," in *2010 IEEE Radar Conference*, pp. 1371–1376, May 2010.

[34] S. Saponara and B. Neri, "Design of compact and low-power X-band radar for mobility surveillance applications," *Computers & Electrical Engineering*, vol. 56, pp. 46–63, 2016.

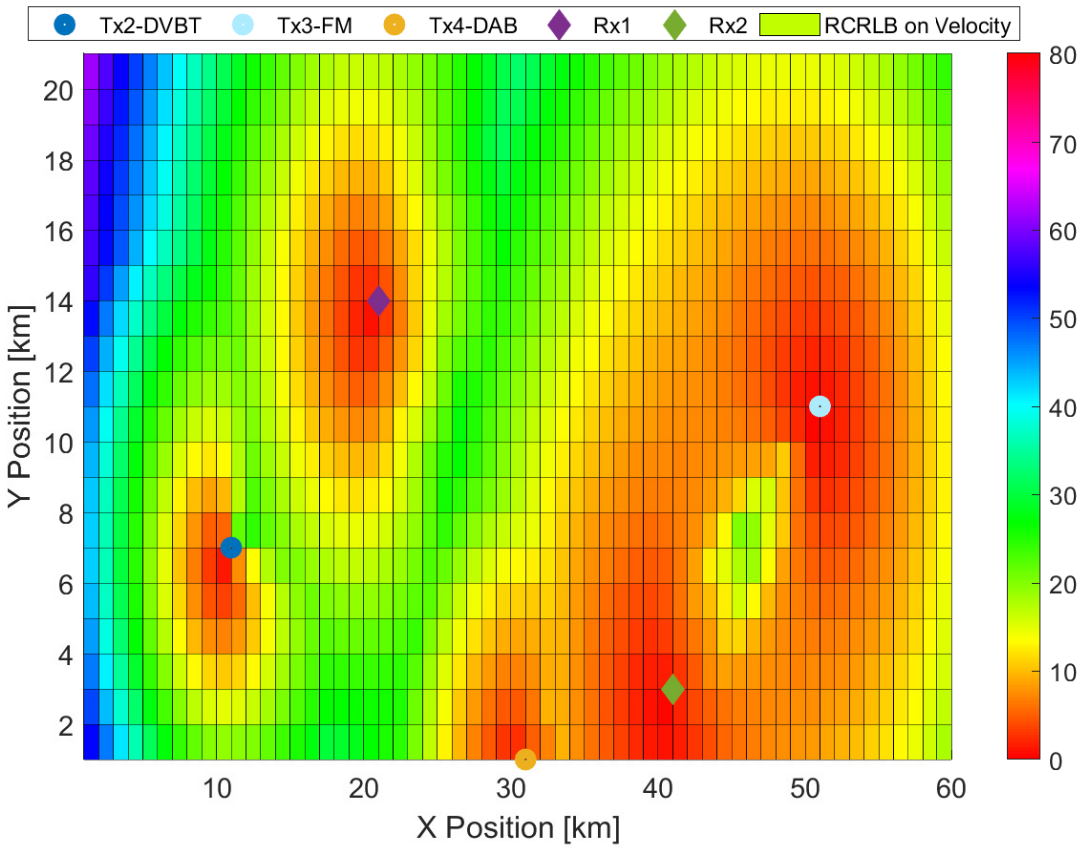

Figure 17: Minimum RCRLBs on velocity of the area of interest surveillanced by multistatic passive radar system in scenario 2.

[35] M. H. Javidan, A. Zaimbashi, and J. Liu, "Target detection in passive radar under noisy reference channel: A new threshold-setting strategy," *IEEE Transactions on Aerospace and Electronic Systems*, vol. 56, pp. 4711–4722, Dec 2020.

[36] G. Cui, J. Liu, H. Li, and B. Himed, "Signal detection with noisy reference for passive sensing," *Signal Processing*, vol. 108, pp. 389–399, 2015.

[37] X. Zhang, H. Li, J. Liu, and B. Himed, "Joint delay and Doppler estimation for passive sensing with direct-path interference," *IEEE Transactions on Signal Processing*, vol. 64, pp. 630–640, Feb 2016.

[38] J. L. Garry, C. J. Baker, and G. E. Smith, "Evaluation of direct signal suppression for passive radar," *IEEE Transactions on Geoscience and Remote Sensing*, vol. 55, pp. 3786–3799, July 2017.

[39] T. Abatzoglou and G. Gheen, "Range, radial velocity, and acceleration MLE using radar LFM pulse train," *IEEE Transactions on Aerospace and Electronic Systems*, vol. 34, pp. 1070–1083, Oct 1998.

[40] T. Tsao, M. Slamani, P. Varshney, D. Weiner, H. Schwarzlander, and S. Borek, "Ambiguity function for a bistatic radar," *IEEE Transactions on Aerospace and Electronic Systems*, vol. 33, pp. 1041–1051, July 1997.

[41] S. D. Blunt and E. L. Mokole, "Overview of radar waveform diversity," *IEEE Aerospace and Electronic Systems Magazine*, vol. 31, pp. 2–42, November 2016.

[42] "Frequency and network planning aspects of DVB-T2," Report EBU-TECH 3348, International Telecommunication Union (ITU), Geneva, May 2011.

[43] H. J. Yardley, "Bistatic radar based on DAB illuminators: The evolution of a practical system," *IEEE Aerospace and Electronic Systems Magazine*, vol. 22, pp. 13–16, Nov 2007.

[44] J. E. Palmer, H. A. Harms, S. J. Searle, and L. Davis, "DVB-T passive radar signal processing," *IEEE Transactions on Signal Processing*, vol. 61, pp. 2116–2126, April 2013.

[45] C. R. Berger, B. Demissie, J. Heckenbach, P. Willett, and S. Zhou, "Signal processing for passive radar using OFDM waveforms," *IEEE Journal of Selected Topics in Signal Processing*, vol. 4, pp. 226–238, Feb 2010.

[46] M. Temiz, E. Alsusa, and M. W. Baidas, "A dual-functional massive MIMO OFDM communication and radar transmitter architecture," *IEEE Transactions on Vehicular Technology*, vol. 69, pp. 14974–14988, Dec 2020.

[47] H. A. Harms, L. M. Davis, and J. Palmer, "Understanding the signal structure in DVB-T signals for passive radar detection," in *2010 IEEE Radar Conference*, pp. 532–537, May 2010.

[48] P. Stinco and F. Gini, "Performance analysis of bistatic radar and optimization methodology in multistatic radar system," *University of Pisa, Pisa*, 2012.

[49] S. Gezici, S. Bayram, M. R. Gholami, and M. Jansson, "Optimal jammer placement in wireless localization networks," in *2015 IEEE 16th International Workshop on Signal Processing Advances in Wireless Communications (SPAWC)*, pp. 665–669, June 2015.